Available online at www.sciencedirect.com

ScienceDirect

journal homepage: www.elsevier.com/locate/he

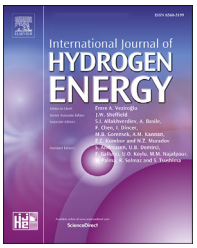

Hydrogen uptake and diffusion kinetics in a quenched and tempered low carbon steel: experimental and numerical study

L.B. Peral [a,b,*], *A. Díaz* [a], *J.M. Alegre* [a], *I.I. Cuesta* [a]

[a] *Universidad de Burgos, Structural Integrity Research Group (GIE), Escuela Politécnica Superior, Avenida Cantabria S/n, 09006, Burgos, España Spain*

[b] *Universidad de Oviedo, SIMUMECAMAT Research Group, Escuela Politécnica Superior de Ingeniería de Gijón, 33203, Gijón, España Spain*

HIGHLIGHTS

- Hydrogen entry is influenced by the charging solution, current density and roughness.
- Apparent diffusion coefficient of hydrogen depends on hydrogen concentration.
- Entry flux is reproduced from HER and absorption theory.
- Finite element framework has been developed to reproduce permeation tests.

ARTICLE INFO

Article history:
Received 2 March 2023
Received in revised form
19 May 2023
Accepted 26 May 2023
Available online xxx

Keywords:
CrMo steel
Surface science
Electrochemistry at surfaces
Hydrogen permeation
Hydrogen trapping and diffusion
Numerical modelling

ABSTRACT

To better understand hydrogen uptake kinetics, electrochemical permeation tests have been performed in a quenched and tempered low-alloy steel. Hydrogen uptake and transport has been studied with three different surface roughness, in four different solutions (1 M H_2SO_4, 1 M H_2SO_4+As_2O_3, 0.1 M NaOH and 3.5% NaCl) and two different hydrogen charging current densities (1 and 5 mA/cm^2). A strong effect of the charging solution, current density and surface roughness has been demonstrated. In 1 M H_2SO_4 + As_2O_3 solution and 5 mA/cm^2, hydrogen recombination on the surface of the samples is strongly reduced and interstitial diffusion prevails due to the trap saturation ($D_L \approx D_{app}$). However, in 1 M H_2SO_4, 0.1 M NaOH and 3.5% NaCl, hydrogen transport is dominated by trapping and detrapping processes ($D_L > D_{app}$). Permeation transients are numerically reproduced through Finite Element simulations and compared to the experimental results. The relationship between hydrogen diffusion kinetics at the microstructural level and surface effects is clearly established by a mapping strategy obtained from the wide range of experimental results, combined with a numerical approach.

* *Corresponding author.*
E-mail addresses: lbperal@ubu.es, luisborja@uniovi.es (L.B. Peral).

https://doi.org/10.1016/j.ijhydene.2023.05.286

Introduction

Hydrogen is postulated as a potential energy carrier to replace fossil fuels and a game changer in the development of the upcoming green economy [1,2]. Nevertheless, a set of mechanical components such as vessels and valves need to be developed for the handling of high-pressure hydrogen gas in preparation for the forthcoming adoption of hydrogen stations. In this regard, chromium–molybdenum steels [3,4] are being postulated as potential candidates to reach a balance between the mitigation of hydrogen embrittlement and manufacturing costs [5,6]. Even though some of these steels are candidates for stationary H_2 storage, susceptibility to hydrogen-related failures can be critical and must be better studied, based on hydrogen adsorption and transport kinetics.

Hydrogen embrittlement (HE) is a phenomenon responsible for unpredictable and premature failure of metallic materials. This type of hydrogen damage is directly related to hydrogen diffusion and trapping phenomena within the material. Interactions between hydrogen atoms and the metallic microstructure are commonly analyzed by Thermal Desorption Analysis [7–9] or using electrochemical hydrogen permeation tests [10–12]. By means of the electrochemical permeation experiments, hydrogen permeability, apparent hydrogen concentration and apparent diffusion coefficient values can be determined [13] to explain the hydrogen/metal interaction. However, hydrogen trapping and diffusion processes can be also influenced by surface processes controlling hydrogen entry. In a liquid solution containing hydrogen species, the entry of hydrogen atoms through the metallic surface is linked to the hydrogen evolution reaction (HER) [12,14]. In this sense, hydrogen adsorption and/or recombination at the surface level is dominated by the hydrogen media, charging current density or surface roughness. Controlling these testing parameters is a key factor to perform a suitable analysis of experimental output data that can be obtained from electrochemical permeation.

A comprehensive analysis of hydrogen diffusion coefficients for a given concentration range needs to be complemented with the accurate determination of hydrogen trapping parameters such as binding energies (E_B) and/or densities of trapping sites (N_T). This characterization for different conditions is crucial to predict how hydrogen can cause damage in metallic components subjected to static and cyclic loads [9,15–22]. The effect of the binding energy and the trap density of a given material state on permeation transients can be modelled through a two-level diffusion equation where the general mass balance for hydrogen in lattice sites is modified by a trapping term [23]; some exact and approximate solutions were firstly derived by McNabb & Foster (1963) [24] for the permeation problem influenced by kinetic trapping. Similarly, Caskey & Pillinger (1975) [25] applied approximate solutions for rise and decay permeation transients to evaluate trapping. However, many authors assume limiting cases for these general solutions, e.g. saturated or diluted traps, to determine N_T and/or E_B [26]. Considering equilibrium between trapped and lattice hydrogen [27], Raina et al. [28] proposed a mapping strategy to determine N_T and E_B from permeation tests at different concentration levels. Nevertheless, the application of this mapping procedure requires a wide range of charging conditions to capture all regimes and relies on the assumption of a constant concentration as a boundary condition on the input side. The relationship between hydrogen uptake and boundary conditions at these very different charging conditions should be better understood to successfully characterize trapping.

In this context, classical approaches to evaluate permeation rely on a simplified modelling in which fickian diffusion and a constant concentration of hydrogen beneath the entry side are assumed. Despite this fitting procedure based on apparent diffusivities and concentrations is still common, the material/hydrogen interaction is not completely defined since hydrogen transport delay due to trapping depends on the concentration regime [29]; additionally, the constant concentration assumption cannot be realistic for some charging conditions [30]. In the present work, trapping effects are accounted for and simulated in a Finite Element 1D framework using the commercial software Comsol Multiphysics. On the other hand, hydrogen uptake is captured through generalized boundary conditions [31] that are derived from HER and absorption/desorption theory.

The goal of this research is to analyze hydrogen uptake and diffusion kinetics through a quenched and tempered low alloy steel using several hydrogen charging solutions and modifying the charging conditions and the surface roughness level. The novelty of this work lies in the combination of experimental and numerical strategies: a complete model accounting for hydrogen evolution reaction, absorption, diffusion and trapping is fed from permeation tests with different electrolytes and charging currents. The wide range of electrolyte conditions facilitates the determination of trapping features using the proposed mapping strategy and therefore the relationship between diffusion phenomena at the microstructural level and the surface effects that take place under different hydrogen charging conditions has been evaluated in a steel grade employed for petrochemical and H_2 applications.

Material

A low-alloyed ferritic steel from the Cr–Mo family has been selected in this study. Table 1 gives the chemical composition. The steel was austenitized at 940 °C for 30 min, quenched in water and finally, tempered at 700 °C for 2 h.

Microstructural characterization was performed by means of a SEM-Jeol-JSM5600 microscope using an acceleration voltage of 20 kV. Previously, samples were ground and polished with diamond paste of 1 μm and finally, etched with Nital 2%. The resulting microstructure, after the aforementioned heat treatment, is shown in Fig. 1. It corresponds to tempered lath martensite, with a prior austenite grain size of 25 μm. The profuse carbide precipitation that takes place during the tempering stage (700 °C for 2 h) can be clearly

Table 1 – Chemical composition (% wt.).

Fe	C	Mn	Si	Cr	Mo
Balance	0.14	0.56	0.16	2.23	1.00

Please cite this article as: Peral LB et al., Hydrogen uptake and diffusion kinetics in a quenched and tempered low carbon steel: experimental and numerical study, International Journal of Hydrogen Energy, https://doi.org/10.1016/j.ijhydene.2023.05.286

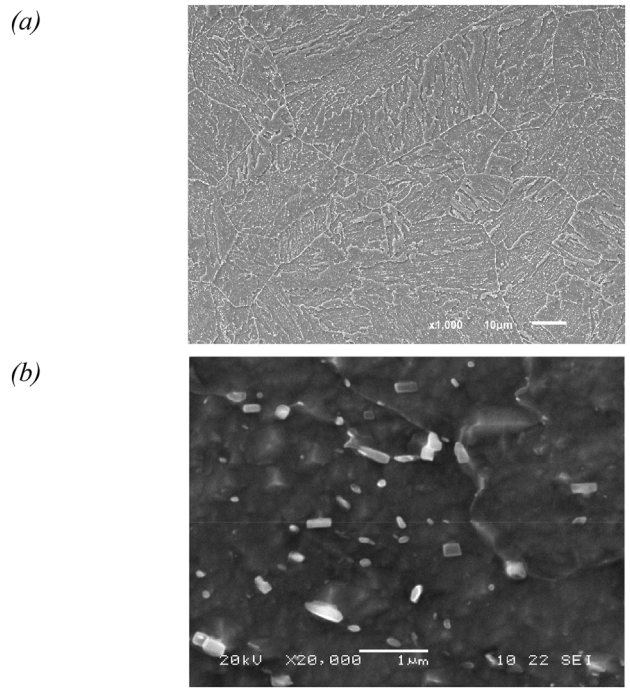

Fig. 1 – SEM. (a) 1000× and (b) 20000×. 2.25Cr1Mo steel grade.

appreciated. These precipitates, distributed along the prior grain boundaries and martensite laths, have been previously identified as M_3C, $M_{23}C_6$ and M_7C_3 [32,33]. As discussed later, these microstructural singularities play an important role on hydrogen trapping and detrapping phenomena.

Experimental procedure

Electrochemical permeation test. Set-up

Fig. 2 displays the experimental set-up of the electrochemical permeation test performed in this study.

Hydrogen atoms are generated on one side of the steel membrane (entry side) and the diffusing hydrogen atoms are oxidized on the other side (exit side). Hence, the current density on the anodic side (hydrogen flow rate) was continuously recorded using an Ivium potentiostat. Samples with a circular area of approximately 1.13 cm^2 and 1 mm thickness were exposed to the solution and the electrochemical tests were conducted at room temperature (~20 °C). Two hydrogen permeation tests were carried out for each case.

The hydrogen entry side was galvanostatically polarized at two different current density levels, $i_c = 1$ and 5 mA/cm^2. Besides, four different solutions were employed: 1 M H_2SO_4 + 0.25 g/l As_2O_3 (pH~1), 1 M H_2SO_4 (pH~1), 0.1 M NaOH (pH~12) and 3.5% NaCl (pH~6.7).

Prior to conducting each electrochemical permeation test, sample surfaces facing the exit side of the double-cell were electrolytically coated with a commercial palladium solution (Je42V solution) that contained 0.2 g/l Pd. Electroplating was performed by applying a current density of 3 mA/cm^2 for 600 s (Fig. 3a). The sample was immediately placed into the double-cell and the Open Circuit Potential (OCP_{Ag/Ag^-Cl}) was monitored in 0.1 M NaOH solution until potential stabilized (Fig. 3b).

After this step, the sample exit side was finally polarized to the final potential monitored during the OCP measurement. In this way, the anodic current density, on the exit side, was stabilized and maintained around 0.1–0.15 $\mu A/cm^2$ before performing the galvanostatic hydrogen cathodic charging.

Roughness measurements

Before permeation testing and after grinding the samples in P120, P600 and P2500 SiC papers, surface roughness was measured by means of an Mitutoyo SJ-210 device. Measurements were done in two random positions and directions over a length of 5 mm using a cut-off length of 0.8 mm following the UNE EN ISO 4287 standard.

Hydrogen evolution reaction (HER)

Electrochemical reactions occurring on the steel surface during cathodic polarization correspond to the hydrogen evolution reaction (HER) comprising an initial electrochemical adsorption (Volmer domain, V), a chemical desorption (Tafel domain, T) and an electrochemical desorption at higher cathodic polarization (Heyrovsky domain, H). These domains are important to analyze the effect of electrochemical adsorption and the competition between adsorption and hydrogen recombination at higher charging current densities.

Potentiodynamic polarization was applied from −600 mV (vs. OCP) at a scan rate of 0.5 mV/s that is enough to preserve quasi-stationary conditions during polarization.

With the aim of modelling hydrogen adsorption and desorption from HER theory, three reactions are considered depending on the electrochemical process involved: adsorption (Volmer), chemical recombination (Tafel) and electrochemical recombination (Heyrovsky). These reactions involve metal sites (M) for hydrogen adsorption, hydrogen protons (H^+), electrons (e^-) and adsorbed hydrogen (MH_{ads}). For acid solutions (HER is given in Fig. 11) the reactions are defined as follows:

$$\text{Adsorption (Volmer): } M + H^+ + e^- \underset{k_{-v}}{\overset{k_v}{\rightleftarrows}} MH_{ads}$$

$$\text{Chemical recombination (Tafel): } MH_{ads} \underset{k_{-t}}{\overset{k_t}{\rightleftarrows}} H_2 + 2M$$

$$\text{Electrochemical recombination (Heyrovsky): } MH_{ads} + H^+ + e^- \underset{k_{-h}}{\overset{k_h}{\rightleftarrows}} H_2 + M$$

where k_v, k_t and k_h are the Volmer, Tafel and Heyrovsky forward reaction constants, respectively. Neglecting the reverse reactions, i.e. those associated to k_{-v}, k_{-t} and k_{-h}, the corresponding current densities can be defined [34] as a charging current, i_c, a chemical recombination current, $i_{r,ch}$ and an electrochemical recombination current, $i_{r,el}$:

Please cite this article as: Peral LB et al., Hydrogen uptake and diffusion kinetics in a quenched and tempered low carbon steel: experimental and numerical study, International Journal of Hydrogen Energy, https://doi.org/10.1016/j.ijhydene.2023.05.286

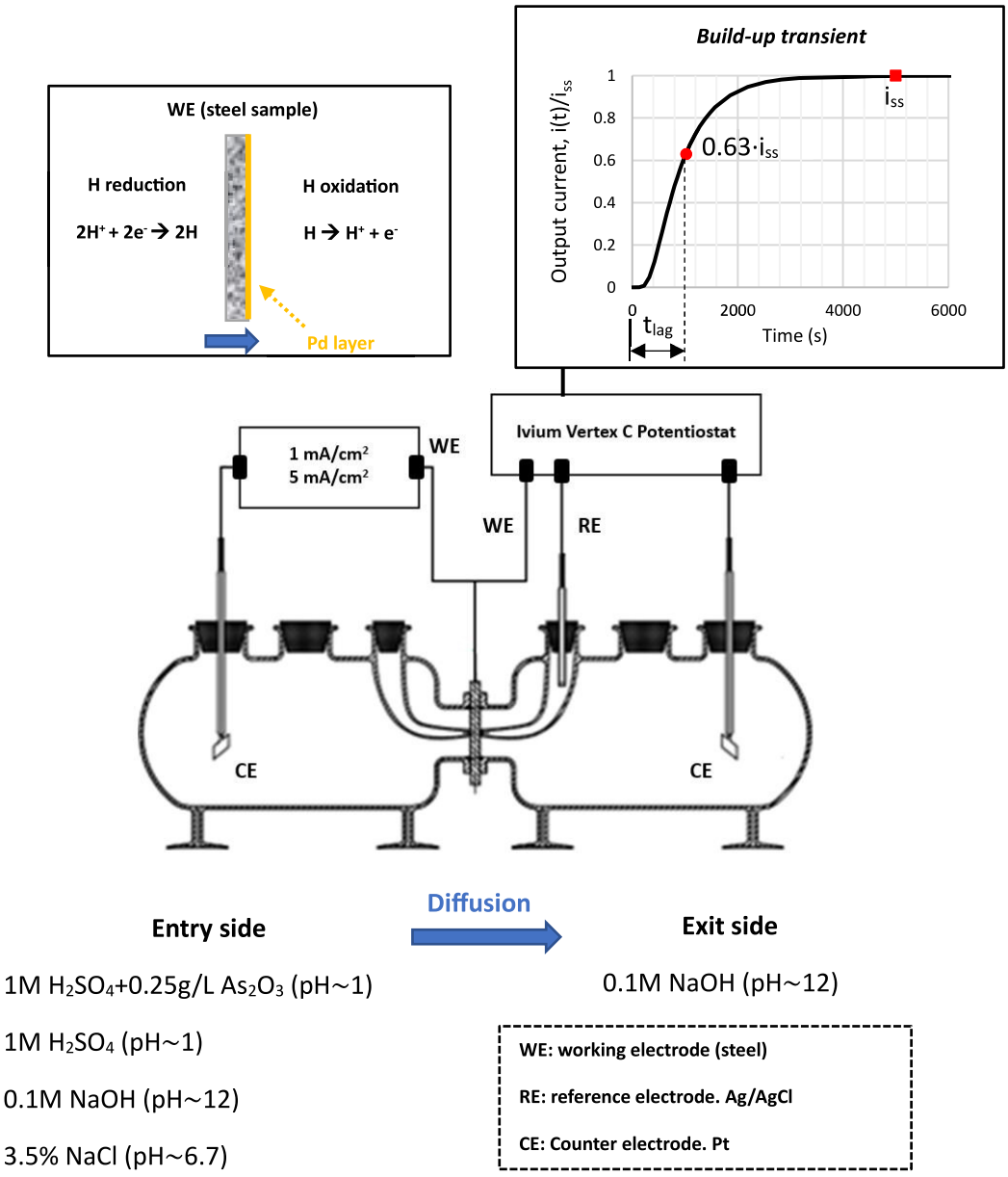

Fig. 2 – Permeation double-cell and test conditions.

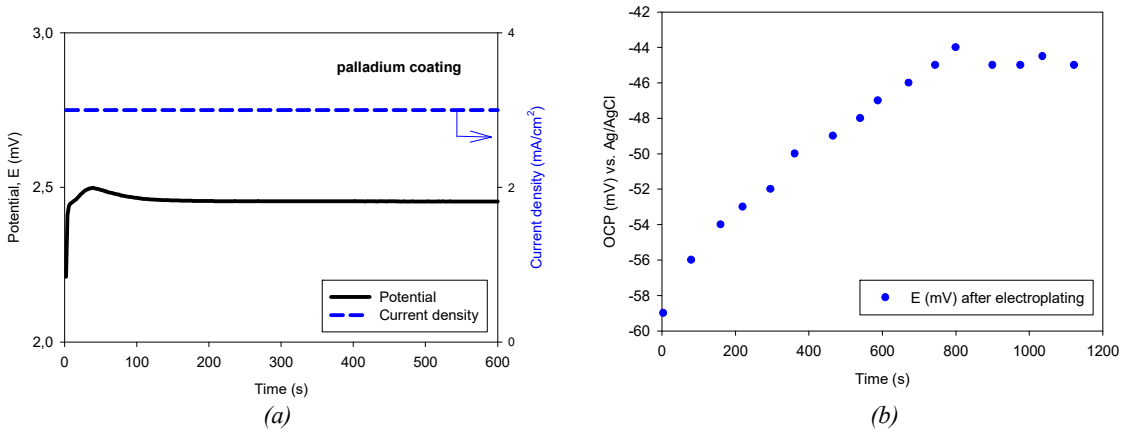

Fig. 3 – (a) Electroplating curve. (b) OCP in NaOH solution after electroplating process with palladium (JE42V solution).

Please cite this article as: Peral LB et al., Hydrogen uptake and diffusion kinetics in a quenched and tempered low carbon steel: experimental and numerical study, International Journal of Hydrogen Energy, https://doi.org/10.1016/j.ijhydene.2023.05.286

$$i_c = 2\Gamma F k_v C_{H^+}(1-\theta_{ad})\exp\left(-\alpha_v\frac{EF}{RT}\right) = Fk_c(1-\theta_{ad}) \quad (1)$$

$$i_{r,ch} = \Gamma F k_t \theta_{ad}^2 = Fk_{r,ch}\theta_{ad}^2 \quad (2)$$

$$i_{r,el} = 2\Gamma F k_h C_{H^+}\theta_{ad}\exp\left(-\alpha_h\frac{EF}{RT}\right) = Fk_{r,el}\theta_{ad} \quad (3)$$

where Γ is the surface concentration of adsorption sites, F the Faraday's constant, C_{H^+} the proton concentration, α_v and α_h the charge transfer coefficients, E the overpotential, R the constant of gases and T the temperature. A surface coverage θ_{ad} is also defined to express the occupancy of adsorption sites while all the other variables are grouped into three constants, k_c, $k_{r,ch}$ and $k_{r,el}$.

Despite these currents are derived from proton-based reactions, the validity can be extended to higher pH where H_2O could be directly involved in HER [35], even though the terms grouped within k_c and $k_{r,el}$ would change. Once hydrogen is adsorbed into the surface, an absorption reaction can be also defined:

$$MH_{ads} \underset{k_{des}}{\overset{k_{abs}}{\rightleftarrows}} MH_{abs}$$

This balance and the corresponding hydrogen fluxes are governed by an absorption constant k_{abs} and a desorption constant k_{des}.

Permeation modelling

To model hydrogen permeation, the numerical problem includes a governing transport equation, i.e. diffusion and trapping, and the corresponding boundary conditions that capture the uptake process.

Diffusion and trapping

The Fick's second law represents a mass balance of the diffusing hydrogen. If the total concentration C drives diffusion:

$$\frac{\partial C}{\partial t} = -\nabla\cdot\mathbf{J} = D_{app}\nabla^2 C \quad (4)$$

where $\mathbf{J}$ is the flux vector and D_{app} is an apparent diffusion coefficient that is independent on concentration and can be fitted from analytical solutions of the diffusion equation. To calculate the apparent diffusivity (D_{app}), the 'time lag' method (equation (5)) was considered [13].

$$D_{app} = \frac{L^2}{6t_{lag}} \quad (5)$$

L is the thickness of the sample ($L = 1$ mm in this study) and t_{lag} is the 'time lag' where $i = 0.63i_{ss}$, being i the measured permeation current density and i_{ss} the permeation current density corresponding to the steady state.

The apparent subsurface concentration, C_{app}, that corresponds to the concentration of hydrogen at the entry side, can be estimated by equation (6) [13], where M_H is the molar mass of hydrogen (1.008 g/mol), F represents the Faraday constant (96,485C/mol) and ρ_{Fe} is the iron density (7.87×10^6 g/m^3). This equation assumes a triangular concentration distribution along the permeation length at the steady state; M_H ρ_{Fe}, and F are included to directly converse output steady state currents into concentrations in wt ppm units. The apparent permeability (P_{app}) is defined according to equation (7).

$$C_{app} = \frac{M_H}{\rho_{Fe}F}\frac{i_{ss}L}{D_{app}} \quad (6)$$

$$P_{app} = C_{app}D_{app} \quad (7)$$

However, it is experimentally demonstrated [36] that the apparent diffusion coefficient increases when a higher concentration level is produced in permeation tests. Therefore, a single D_{app} value does not characterize hydrogen diffusion through the material. This is caused by trapping effects: microstructural defects retain the diffusing hydrogen atoms and delay permeation, but this effect is weaker for high concentrations since traps are rapidly filled. To model these phenomena in permeation, the mass balance is modified to include both lattice hydrogen, C_L, and trapped hydrogen, C_T:

$$\frac{\partial C_L}{\partial t} + \frac{\partial C_T}{\partial t} = -\nabla\cdot\mathbf{J}_L = D_L\nabla^2 C_L \quad (8)$$

In that balance the flux term is considered to be driven only by gradients in C_L and therefore the ideal lattice diffusivity D_L must be known. Assuming thermodynamic equilibrium between C_L and C_T, the governing equation is rearranged as follows [37]:

$$\frac{\partial C_L}{\partial t} + \frac{K_T N_T/N_L}{\left[1+(K_T-1)C_L/N_L\right]^2}\frac{\partial C_L}{\partial t} = D_L\nabla^2 C_L \quad (9)$$

where N_T is the density of trapping sites, N_L the density of lattice sites, and the equilibrium constant K_T can be expressed through an Arrhenius function of the trap binding energy E_B, i.e. $K_T = \exp(E_B/RT)$. For the numerical simulation of permeation curves, Section 4.3, this equation is implemented in the commercial finite element software Comsol Multiphysics 6.0 using the *Transport of Diluted Species* module. Trapping effects are modelled adding a reaction term in the governing mass balance. The permeation slab is simulated by a 1D model with 10^4 elements; this mesh density was chosen after a sensitivity study and a linear discretization is selected for the solved dependent variable, i.e. for C_L . For all the analyzed cases, an empty initial condition is assumed ($C_L = 0$ for all nodes at $t = 0$) and two different boundary conditions are modelled for the entry and exit nodes: a generalized flux accounting for electrochemical adsorption/absorption is imposed in the entry node whereas a zero concentration boundary condition is fixed in the exit node to reproduce instantaneous hydrogen oxidation in the detection permeation cell. Mathematical approaches to model dynamic boundary conditions to reproduce non-instantaneous hydrogen desorption have been proposed by Zaika et al. [38,39] but are out of the scope of the present work.

Uptake

The usual constant concentration assumption for the boundary condition of the hydrogen transport problem is only valid under some conditions: (i) for hydrogen entry from a

Please cite this article as: Peral LB et al., Hydrogen uptake and diffusion kinetics in a quenched and tempered low carbon steel: experimental and numerical study, International Journal of Hydrogen Energy, https://doi.org/10.1016/j.ijhydene.2023.05.286

gaseous H_2 environment when the dissociation reaction is in equilibrium, which results in the Sievert's law for the boundary concentration; (ii) for electrochemical uptake when the absorption/desorption reactions are much faster than diffusion, as discussed below. A more general condition for modelling hydrogen entry is based on the definition of an entry flux J_{in} from the balance of three phenomena: electrochemical generation/recombination (HER: hydrogen evolution reaction), intermediate absorption/desorption (HAR: hydrogen absorption reaction) and the diffusion of absorbed hydrogen through the lattice sites.

$$J_{in} = J_{HER} = J_{HAR} = J_L \tag{10}$$

The relationship between these three processes can be used to define a general flux that depends on the evolution of the surface concentration, i.e. the proposed generalized boundary conditions does not necessarily result in a constant flux or a constant concentration in the entry surface. Therefore, the flux boundary condition is implemented in the Finite Element code as:

$$\mathbf{J}_L \cdot \mathbf{n} = J_{in} \tag{11}$$

where n is the unitary vector normal to the entry surface. From the HER theory previously presented, a flux of hydrogen atoms adsorbing to the metal surface can be expressed as [34]:

$$J_{HER} = \Gamma \frac{\partial \theta_{ad}}{\partial t} = \frac{1}{F}(i_c - i_{r,ch} - i_{r,el}) \tag{12}$$

and substituting the current densities for charging and recombination:

$$J_{HER} = k_c(1-\theta_{ad}) - k_{r,ch}\theta_{ad}^2 - k_{r,el}\theta_{ad} \tag{13}$$

This means that k_c, $k_{r,ch}$ and $k_{r,el}$ have flux units, e.g. mol/(m^{2}s).

On the other hand, the adsorbed hydrogen enters as an absorbed atom to the first layers of lattice sites and the surface coverage, θ_{ad}, can be related to the boundary lattice concentration, C_L^0.

A flux can be simply expressed as the sum of the absorption flux, proportional to the number of empty lattice and to the proportion of adsorbed hydrogen, and a desorption flux, proportional to the number of empty sites and to the lattice hydrogen.

$$J_{HAR} = k_{abs}N_L(1-\theta_L)\theta_{ad} - k_{des}C_L^0(1-\theta_{ad}) \tag{14}$$

For low-solubility alloys:

$$J_{HAR} = k_{abs}N_L\theta_{ad} - k_{des}C_L^0(1-\theta_{ad}) \tag{15}$$

It must be noted that a concentration of sites must be included in the absorption term so desorption and absorption constants have the same units. Here, N_L is included in the absorption term so both k_{abs} and k_{des} have velocity units, e.g. m/s. In contrast, the absorption constant in literature [40] usually takes the dimension of a flux, e.g. mol/(m^{2}s) since the concentration of sites is omitted.

Hydrogen uptake is modelled in Comsol Multiphysics by including an input flux in the entry node $J_{in} = J_{HER}$. However, θ_{ad} must be determined in each iteration as a function of C_L^0, which is not constant and depends on hydrogen entry and diffusion. The flux equality condition, $J_{HER} = J_{HAR}$ is operated to establish a second-order equation for θ_{ad}:

$$k_{r,ch}\theta_{ad}^2 + (k_{abs}N_L + k_{des}C_L^0 + k_c + k_{r,el})\theta_{ad} - k_{des}C_L^0 - k_c = 0 \tag{16}$$

For the sake of simplicity, recombination is assumed to be governed only by the Tafel step, and therefore $k_{r,el} = 0$, as in Ref. [40], during constant fitting and numerical simulation of permeation. To obtain k_{abs}, k_{des}, k_c and $k_{r,ch}$, a strategy is proposed that relies in two conditions.

Condition 1. Absorption and desorption processes occur much faster than bulk diffusion, i.e. the problem is diffusion-controlled. In these cases, $J_{in} \ll N_L k_{abs}$ and $J_{in} \ll N_L k_{des}$. Assuming that $J_{in} = J_{HAR}$:

$$\frac{J_{in}}{N_L k_{des}} = \frac{k_{abs}}{k_{des}}\theta_{ad} - \frac{C_L^0}{N_L}(1-\theta_{ad}) \approx 0 \tag{17}$$

Therefore, a relationship between surface concentration in the entry side, C_L^0, and the coverage of adsorbed hydrogen, θ_{ad}, can be established as a function of the ratio $\kappa_{HAR} = k_{abs}/k_{des}$:

$$C_L^0 = N_L \kappa_{HAR} \frac{\theta_{ad}}{1-\theta_{ad}} \tag{18}$$

Condition 2. HER reactions take place faster than diffusion and thus $J_{in} \ll k_c$ and $J_{in} \ll k_{r,ch}$. Assuming that $J_{in} = J_{HER}$:

$$\frac{J_{HER}}{k_{r,ch}} = \frac{k_c}{k_{r,ch}}(1-\theta_{ad}) - \theta_{ad}^2 \approx 0 \tag{19}$$

This condition implies that θ_{ad} only depends on the relationship between HER constants, i.e. on the ratio $\kappa_{HER} = k_c/k_{r,ch}$.

Results and discussion

Experimental permeation curves

Influence of surface roughness on hydrogen permeation

The influence of the surface roughness on the hydrogen permeation has been studied under three different roughness levels (Fig. 4). Two permeation tests were conducted on each

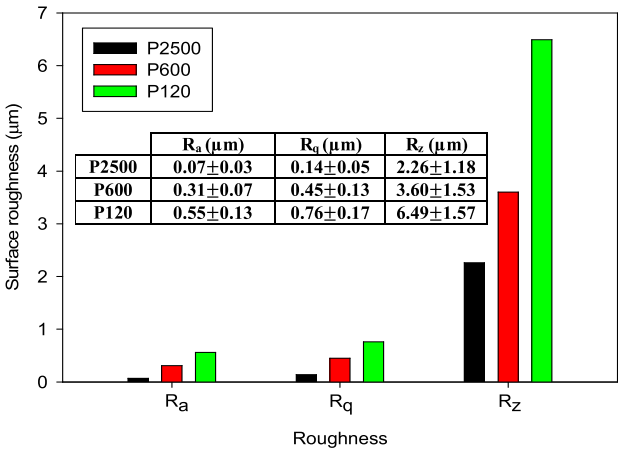

	R_a (µm)	R_q (µm)	R_z (µm)
P2500	0.07±0.03	0.14±0.05	2.26±1.18
P600	0.31±0.07	0.45±0.13	3.60±1.53
P120	0.55±0.13	0.76±0.17	6.49±1.57

Fig. 4 – Surface roughness measurements.

Please cite this article as: Peral LB et al., Hydrogen uptake and diffusion kinetics in a quenched and tempered low carbon steel: experimental and numerical study, International Journal of Hydrogen Energy, https://doi.org/10.1016/j.ijhydene.2023.05.286

surface roughness condition. R_a is the arithmetic average of the deviations of the roughness profile from the centerline along the evaluation length, R_q represents the quadratic average of the deviations of the roughness profile from the midline and R_z is the arithmetic mean of all the peak-valley values of the profile.

The electrochemical hydrogen permeation curves are displayed in Fig. 5 whilst the experimental permeation data, obtained from these curves, are given in Table 2.

On the basis of the obtained results, hydrogen maximum flux, i.e. the steady state output current (i_{ss}), decreases and the observed time lag (t_{lag}) is higher as surface roughness increases. It is important to highlight that this effect was more pronounced when the average surface roughness (R_a) increased to 0.56 μm (P120 state). In this case, the hydrogen apparent concentration (C_{app}) and the apparent diffusivity (D_{app}) were considerably lower (Fig. 6). This fact was also reported in Ref. [41]. As discussed later, as surface roughness increases, hydrogen recombination on the surface of the permeated sample also increases ($k_{r,ch}$, Table 5) and consequently, the apparent hydrogen diffusivity is reduced because the concentration level decreases and thus the occupancy of hydrogen trapping sites is lower. However, P2500 and P600 states have evidenced a higher apparent hydrogen diffusion coefficient, close to the lattice <interstitial> diffusion coefficient ($D_L = 2 \times 10^{-10}$ m^2/s, Table 4). In this case, a higher apparent hydrogen concentration is introduced (~ 6 wt ppm), by virtue of the lower chemical recombination (Table 5) on the hydrogen entry surface of the samples, which causes the traps to be saturated and therefore, D_{app} is more similar to D_L.

Despite the modelling approach previously presented for hydrogen uptake is based on generalized boundary conditions, the determination of apparent diffusivities from experimental permeation transients requires the assumption of constant concentration or constant flux conditions in the entry side. As discussed in Section 4.2, a constant input flux is reached much later than a constant surface concentration, and thus the t_{lag} expression in Tables 2 and 3.

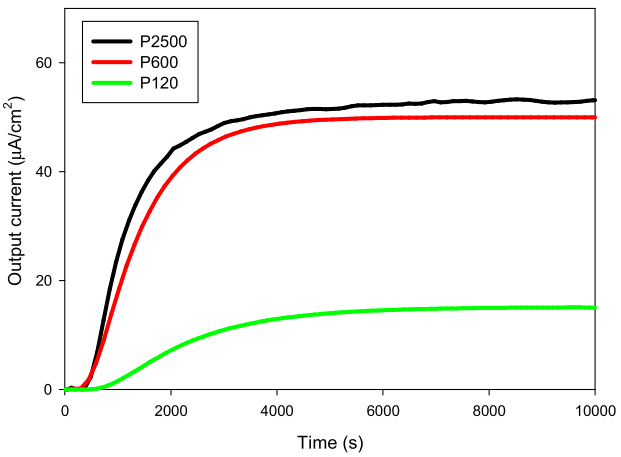

Fig. 5 – Roughness influence on hydrogen permeation. Hydrogen charging in 1 M H_2SO_4 + 0.25 g/L As_2O_3 with a charging current of 1 mA/cm^2.

Influence of current density and charging solution on hydrogen permeation

Figs. 7 and 8 demonstrate the influence of the charging current density (i_c = 1 and 5 mA/cm^2, respectively) on the electrochemical hydrogen permeation, with four different hydrogen charging solutions.

Results obtained from Figs. 7 and 8 are summarized in Table 3. As expected, the current density level for hydrogen generation on the entry side notably influenced hydrogen permeability. As current level increases from 1 to 5 mA/cm^2, the hydrogen flux (i_{ss}), the subsurface hydrogen concentration (C_{app}) and the apparent diffusivity (D_{app}) also increase (Figs. 9 and 10).

Hydrogen permeation flux considerably increases when permeation tests are carried out with 1 M H_2SO_4 + 0.25 g/L AsO_3 (pH~1). Due to the As_2O_3 addition, hydrogen recombination on the entry side is partially mitigated (Fig. 16) and consequently, a higher hydrogen concentration is introduced (Table 3 and Fig. 9).

Regarding the apparent diffusion coefficient, diffusivity increases under 5 mA/cm^2 due to the higher trap occupancy [11,12]. Besides, the plot of D_{app} as a function of the hydrogen charging solution (Fig. 10) evidences two domains: in domain (1), with a maximum value of 1.8×10^{-10} m^2/s for a subsurface concentration of about 10 wt ppm, interstitial diffusion seems to predominate because traps are close to be filled. This fact is later reported in Fig. 15. The higher trapping effect is also shown in Fig. 8, since the slope of the permeation transient notably increases. In this case, we can presume that hydrogen trapping sites are almost full because interstitial diffusivity (2×10^{-10} m^2/s in Table 4) and the apparent diffusivity are almost equal. Therefore, interstitial diffusivity prevails. However, domain (2) is linked to the stronger hydrogen trapping effects in a more diluted regime.

As discussed below by means of the fitting procedure for HER parameters, recombination constant increases when As_2O_3 is removed from the hydrogen charging solution (Table 6 and Table 7). Accordingly, when permeation experiments are carried out in 1 M H_2SO_4 solution, the subsurface hydrogen concentration decreases (Figs. 9 and 16) in comparison to 1 M H_2SO_4 + 0.25 g/l As_2O_3 both 1 (Volmer region, V) and 5 mA/cm^2 (Volmer + Heyrovsky region, V + H), Fig. 11.

From Fig. 11, two different domains are identified by representing $d\ln|i|/dE$ as a function of the potential (E). The first one, for cathodic potentials lower than −450 $mV_{Ag/AgCl}$, corresponds to the electrochemical adsorption step (Volmer domain). The second one, for cathodic potentials above −800 $mV_{Ag/AgCl}$, corresponds to the electrochemical or chemical desorption step (Heyrovsky and Tafel reactions). These domains are distinguished by the evolution of $d\ln|i|/dE$ that takes a constant value in the aforementioned domains (Fig. 11). The identification of domains is based on the work of Frappart et al. [12]. These points are important to distinguish later the effect of electrochemical adsorption and the competition between adsorption/desorption, as previously described in section 3.3. The numerical simulation of the experimental permeation curves includes generalized boundary conditions that reproduce hydrogen uptake as a function of constants (absorption/desorption) linked to these different reaction mechanisms.

Please cite this article as: Peral LB et al., Hydrogen uptake and diffusion kinetics in a quenched and tempered low carbon steel: experimental and numerical study, International Journal of Hydrogen Energy, https://doi.org/10.1016/j.ijhydene.2023.05.286

Table 2 – Experimental data obtained from electrochemical permeation tests in Fig. 5.

Grinding	i_c (mA/cm^2)	i_{ss} (μA/cm^2)	t_{lag} (s) in 0.63 i_{ss}	D_{app} (m^2/s)	C_{app} (wt ppm)	P_{app} (molH/m·s)
P2500 (R_a = 0.07 μm)	1	54.8	1410	1.2×10^{-10}	6.1	2.8×10^{-9}
P600 (R_a = 0.31 μm)		50.0	1540	1.1×10^{-10}	6.0	2.6×10^{-9}
P120 (R_a = 0.56 μm)		15.1	2540	6.6×10^{-11}	3.0	7.7×10^{-10}

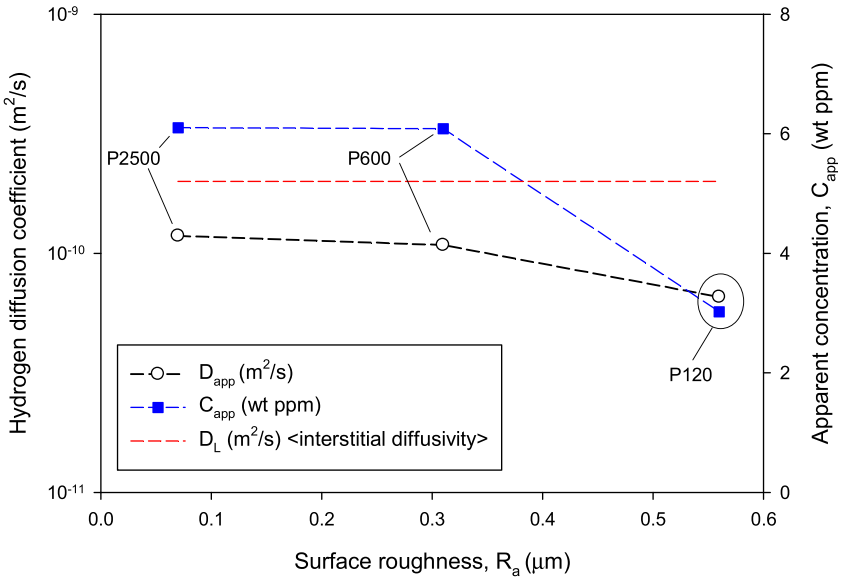

Fig. 6 – Influence of surface roughness of the apparent concentration (C_{app}) and apparent diffusivity (D_{app}).

Table 3 – Experimental data obtained from electrochemical permeation tests.

Hydrogen charging solution	i_c (mA/cm^2)	i_{ss} (μA/cm^2)	t_{lag} (s) in 0.63 i_{ss}	D_{app} (m^2/s)	C_{app} (wt ppm)	P_{app} (molH/m·s)
1 M H_2SO_4 + 0.25 g/L As_2O_3	1	54.8	1410	1.2×10^{-10}	6.1	2.8×10^{-9}
	5	135.9	930	1.8×10^{-10}	10.0	7.0×10^{-9}
1 M H_2SO_4	1	14.3	4430	3.8×10^{-11}	5.0	7.3×10^{-10}
	5	27.9	3820	4.4×10^{-11}	8.5	1.5×10^{-9}
0.1 M NaOH	1	8.6	4930	3.1×10^{-11}	3.5	4.2×10^{-10}
	5	18.1	3918	4.3×10^{-11}	5.6	9.3×10^{-10}
3.5% NaCl	1	3.5	3685	4.5×10^{-11}	1.0	1.8×10^{-10}
	5	5.4	3400	5.0×10^{-11}	1.5	2.8×10^{-10}

Table 4 – Experimental data obtained from Figs. 12–14.

Transient	i_{ss} (μA/cm^2)	0.63 i_{ss} (μA/cm^2)	time lag (s)	D_{app} (m^2/s)	D_L (m^2/s)	C_{app} (wt ppm)	N_T from eq. (20) (sites/m^3)
1st	15.15	9.54	2530	6.6×10^{-11}	2×10^{-10}	3.0	–
2nd	14.98	9.44	1320	1.3×10^{-10}		1.6	7.1×10^{23}

Table 5 – Influence of surface roughness on uptake constants.

1 M H_2SO_4 + 0.25 g/L As_2O_3; i_c = 1 mA/cm^2

Grinding	i_{ss} (μA/cm^2)	C_L^0 (wt ppm)	$k_{r,ch}$ mol/(m^{2}s)	k_c mol/(m^{2}s)	κ_{HER}	θ_{ad}
P2500 (R_a = 0.07 μm)	54.8	3.61	1.58×10^{-3}	5.45×10^{-4}	3.45	0.81
P600 (R_a = 0.31 μm)	50.0	3.29	1.64×10^{-3}	5.07×10^{-4}	3.09	0.80
P120 (R_a = 0.56 μm)	15.1	0.99	3.55×10^{-3}	2.25×10^{-4}	0.63	0.54

Regarding the basic solutions, the apparent hydrogen concentration (C_{app}) decreases in 0.1 M of NaOH solution and especially, in 3.5% of NaCl (Fig. 9) where the surface chemical recombination constant is notably higher, Fig. 16. Hence, occupancy of lattice sites on the entry side (θ_L^0) is considerably lower, Fig. 15.

Please cite this article as: Peral LB et al., Hydrogen uptake and diffusion kinetics in a quenched and tempered low carbon steel: experimental and numerical study, International Journal of Hydrogen Energy, https://doi.org/10.1016/j.ijhydene.2023.05.286

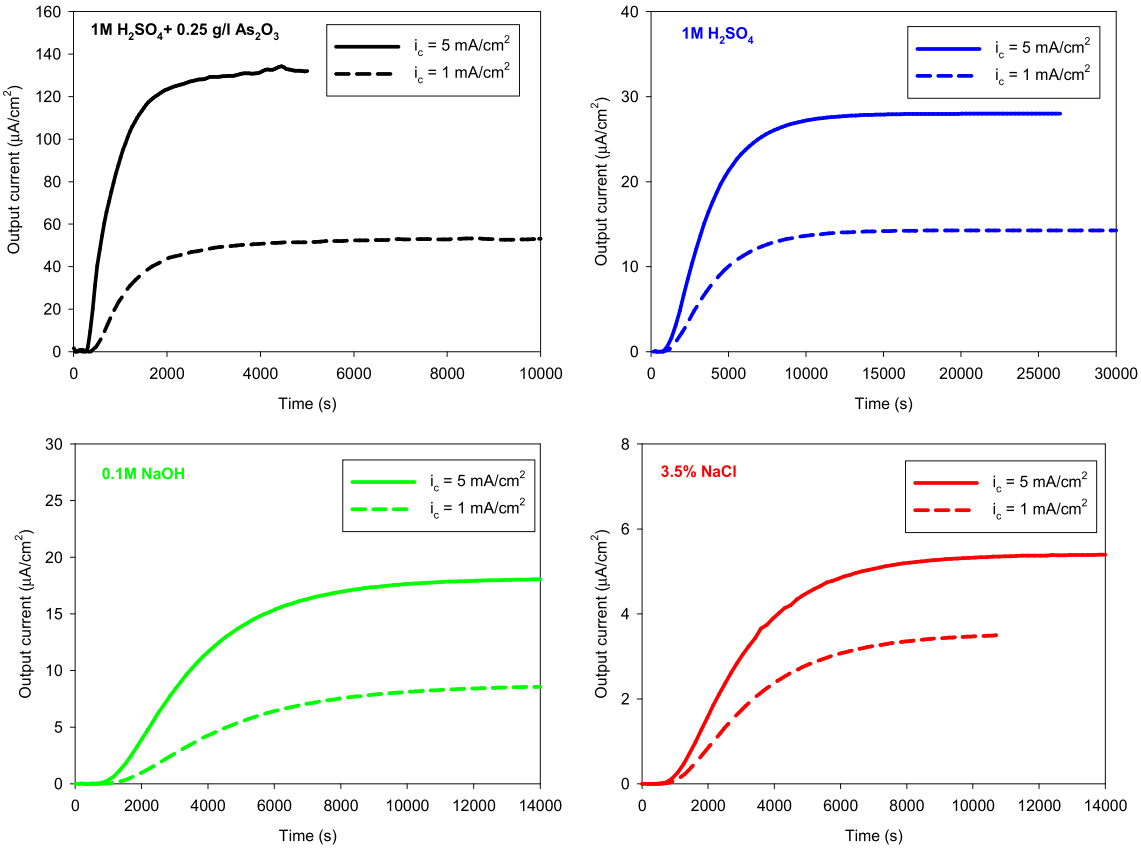

Fig. 7 – Influence of the current density level (i_c) on the hydrogen permeation. Surface Grinding: P2500.

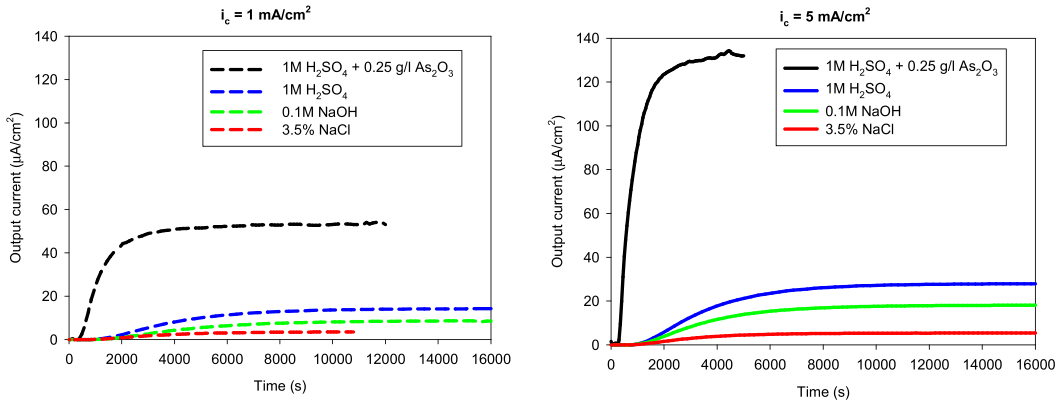

Fig. 8 – Influence of the hydrogen charging solution on the hydrogen permeation at 1 and 5 mA/cm^2. nSurface Grinding: P2500.

Diffusible and trapped hydrogen

To further analyze trapping and detrapping phenomena, two consecutive hydrogen permeations tests were carried out to attain higher occupancy of hydrogen traps. Permeation curves are shown in Figs. 12 and 13 while permeation data, obtained from these curves, are summarized in Table 4.

Surface roughness: P120. Solution: 1 M H_2SO_4 + 0.25 g/l As_2O_3. Current density: 1 mA/cm^2

Equation (20) can be used to determine the density of traps (N_T) in the steel microstructure through the direct application of the values of the diffusivity and the concentration of the subsurface when traps occupancy is high ($\theta_T = 1$) [12].

$$N_T = \frac{C_{app}}{3}\left(\frac{D_L}{D_{app}} - 1\right) \quad (20)$$

Lattice diffusion coefficient (D_L) can be estimated from the decay transient after switching-off the hydrogen generation current in the entry side [42,43]. In the initial part of the discharge curve (Fig. 14), desorption of lattice diffusible hydrogen governs the output flux and this part of the curve is

Please cite this article as: Peral LB et al., Hydrogen uptake and diffusion kinetics in a quenched and tempered low carbon steel: experimental and numerical study, International Journal of Hydrogen Energy, https://doi.org/10.1016/j.ijhydene.2023.05.286

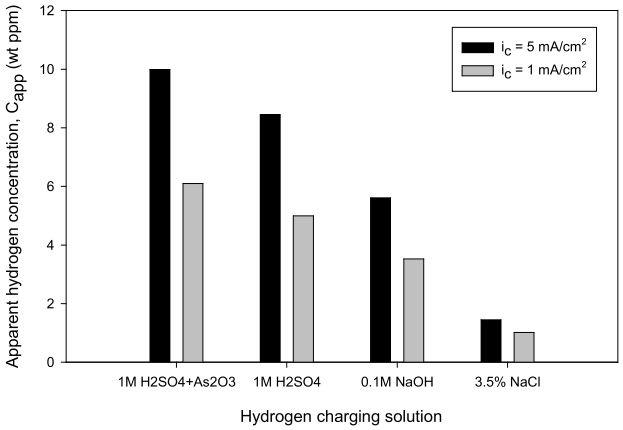

Fig. 9 – Influence of current density and hydrogen charging solution on the apparent hydrogen concentration (C_{app} in wt ppm).

well described by the analytical solution of Fick's law for permeation assuming a constant concentration on the entry side (equation (21)).

$$\frac{J(t)}{J_{ss}} = 1 - \frac{2}{\sqrt{\pi\tau}} \sum_{n=0}^{\infty} \exp\left[-\frac{(2n+1)^2}{4\tau} \right] \tag{21}$$

$$\tau = \frac{D_L t}{L^2} \tag{22}$$

In addition, the complete decay can be used to quantify the lattice hydrogen concentration along the slab and the reversible trapped hydrogen, by analyzing the area under the curve. The area, 'A_i', in $\mu A \cdot s/cm^2$, defined between experimental and theoretical lattice diffusivity, corresponds to the amount of reversible trapped hydrogen (C_{rev}) in the steel microstructure. This area can be converted in hydrogen 'wt ppm' units using the equation (23). On the other hand, the area under the theoretical lattice diffusivity corresponds to the lattice hydrogen content (i.e. interstitial hydrogen).

$$C_H = A_i \frac{M_H}{F L \rho_{Fe}} \tag{23}$$

Additionally, it is also possible to estimate the amount of irreversible trapped hydrogen (C_{irrev}) by assuming that, when a palladium coating has been deposited on the exit side, total hydrogen content into the steel membrane is not homogeneous but follows a linear distribution along the thickness, and the average total concentration can be approximated by $\langle C \rangle \approx C_{app}/2$ [12].

$$C_{irrev} = \langle C \rangle - C_L - C_{rev} \tag{24}$$

From Fig. 14, interstitial hydrogen content (C_L) was found to be 0.17 wt ppm while the reversible trapped (C_{rev}) is 0.38 wt ppm. From these values and taking the average hydrogen concentration obtained from the first permeation with $\langle C \rangle$ equal to 1.5 wt ppm, the irreversible trapped hydrogen content is 0.95 wt ppm.

Ferrite/carbides interfaces and martensite laths and packets (Fig. 1) can act as potential reversible hydrogen trapping sites [9,44], temporarily capturing the aforementioned reversible hydrogen content. Besides, irreversible trapped content is mainly attributed to hydrogen trapped in prior grains boundaries and dislocations core [10,12]. Accordingly, the ratios of each hydrogen species are $C_L \approx 11\%$, $C_{rev} \approx 25\%$ and $C_{irrev} \approx 64\%$. Hydrogen retention on these trapping sites influences diffusion kinetics, as previously demonstrated in Fig. 10.

On the other hand, a second permeation transient was performed to evaluate the density of traps (N_T) by means of equation (20). Trapping density, $N_T = 7.1 \times 10^{23}$, was only estimated after the second permeation transient, when interstitial diffusivity prevails ($D_{app} \approx D_L$) due to the higher occupancy of the hydrogen trapping sites on the entry side. As already mentioned, equation (20) presents some limitations: it represents a limiting case for saturated traps and hence it can be only used when trap occupancy is high ($\theta_T = 1$). On the other hand, the solution derived originally [24] did not

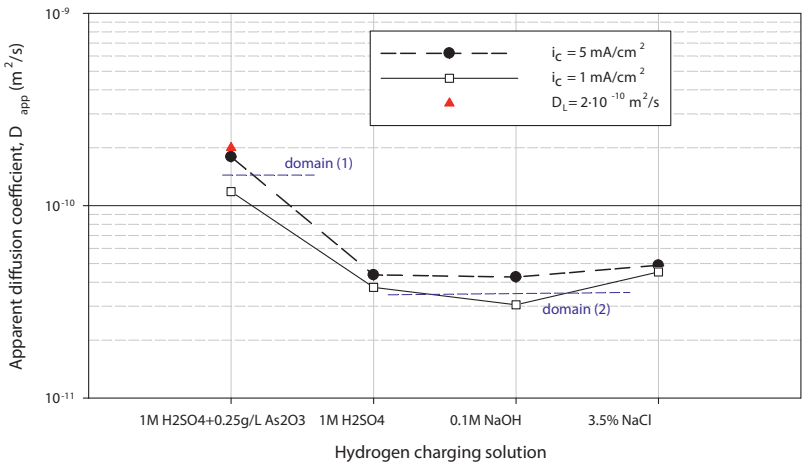

Fig. 10 – Influence of current density and hydrogen charging solution on the apparent hydrogen diffusivity (D_{app} in m^2/s).

Please cite this article as: Peral LB et al., Hydrogen uptake and diffusion kinetics in a quenched and tempered low carbon steel: experimental and numerical study, International Journal of Hydrogen Energy, https://doi.org/10.1016/j.ijhydene.2023.05.286

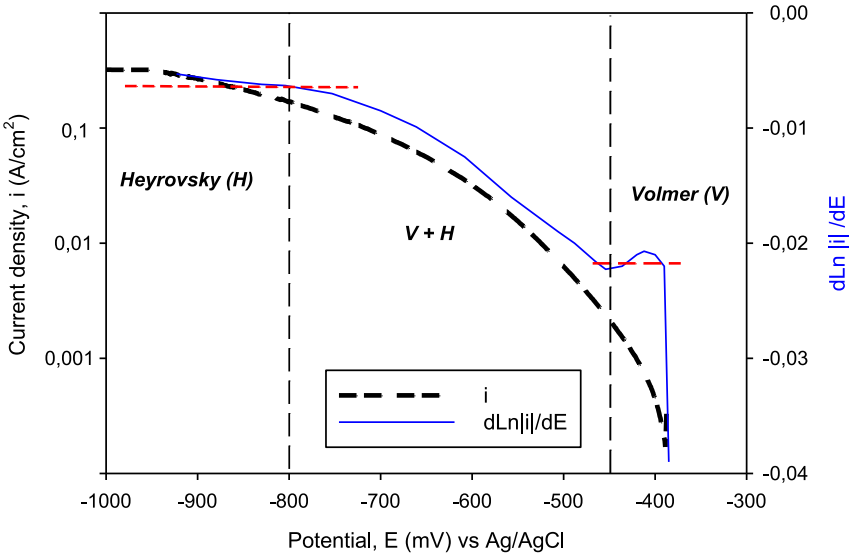

Fig. 11 – Hydrogen evolution reaction (HER) in an acid aqueous solution (1 M H_2SO_4).

Table 6 – Influence of charging solution on uptake constants for $i_c = 1$ mA/cm².

$i_c = 1$ mA/cm²; P2500						
Solution	i_{ss} (μA/cm²)	C_L^0 (wt ppm)	$k_{r,ch}$ mol/(m²s)	k_c mol/(m²s)	κ_{HER}	θ_{ad}
1 M H_2SO_4 + 0.25 g/l As_2O_3	54.77	3.61	1.58×10^{-4}	5.45×10^{-4}	3.45	0.81
1 M H_2SO_4	14.27	0.94	3.75×10^{-4}	2.19×10^{-4}	0.58	0.53
0.1 M NaOH	8.60	0.54	6.87×10^{-4}	1.69×10^{-4}	0.25	0.39
3.5% NaCl	3.49	0.23	2.27×10^{-3}	1.32×10^{-4}	0.06	0.21

Table 7 – Influence of charging solution on uptake constants for $i_c = 5$ mA/cm².

$i_c = 5$ mA/cm²; P2500						
Solution	i_{ss} (μA/cm²)	C_L^0 (wt ppm)	$k_{r,ch}$ mol/(m²s)	k_c mol/(m²s)	κ_{HER}	θ_{ad}
1 M H_2SO_4 + 0.25 g/l As_2O_3	134.05	8.83	6.22×10^{-4}	5.92×10^{-3}	9.51	0.91
1 M H_2SO_4	29.92	1.97	1.06×10^{-3}	1.72×10^{-3}	1.63	0.70
0.1 M NaOH	18.11	1.19	1.52×10^{-3}	1.25×10^{-3}	0.82	0.59
3.5% NaCl	5.40	0.36	5.92×10^{-3}	7.36×10^{-4}	0.12	0.30

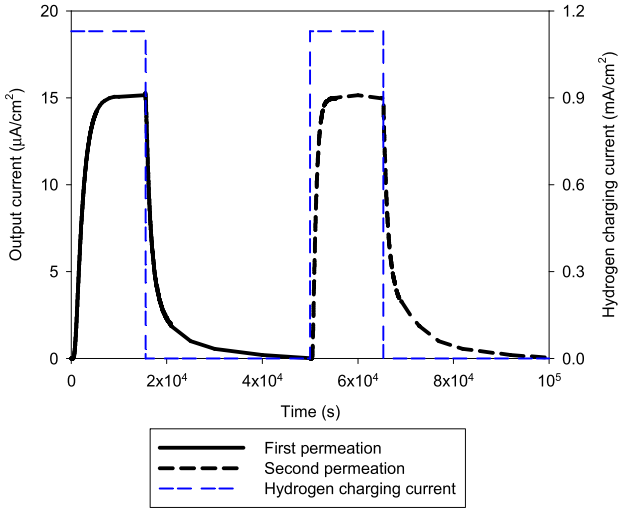

Fig. 12 – Hydrogen permeation transients.

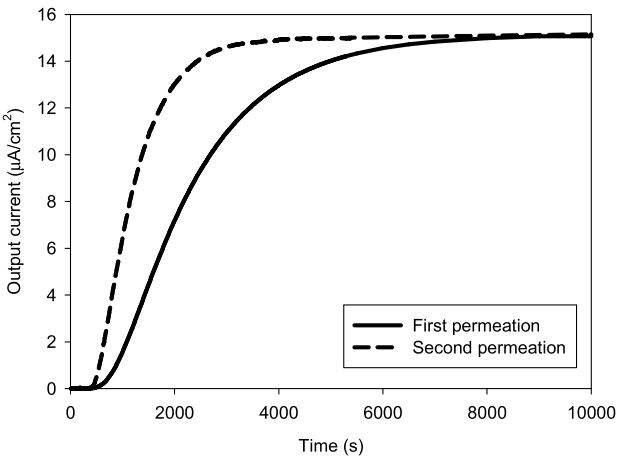

Fig. 13 – Comparison between the first and second hydrogen permeation transients.

Please cite this article as: Peral LB et al., Hydrogen uptake and diffusion kinetics in a quenched and tempered low carbon steel: experimental and numerical study, International Journal of Hydrogen Energy, https://doi.org/10.1016/j.ijhydene.2023.05.286

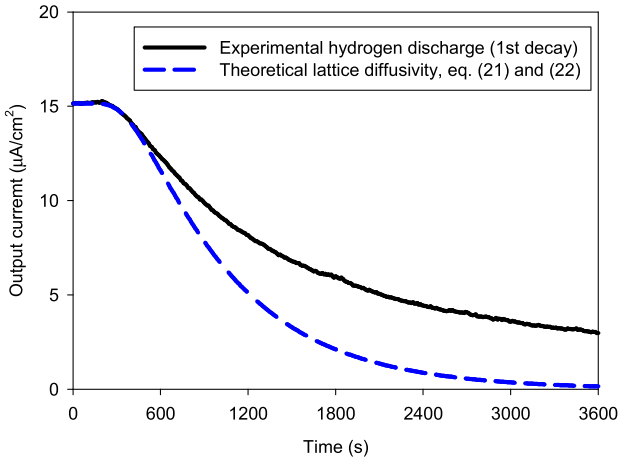

Fig. 14 – Lattice diffusivity estimation from the decreasing permeation transient.

included C_{app} but the boundary concentration C_L^0, as also found by Raina et al. [28] through an asymptotic analysis.

Therefore, to better capture trapping effects at different concentration regimes, the mapping strategy to fit K_T and N_T from permeation results is here followed. In this case, different concentrations in the entry side, and thus lattice occupancies θ_L^0, are not only obtained by varying the charging current but also with different charging solutions.

The analytical expression derived by McNabb and Foster (1963) [24] is then used to fit all the experimental pairs $D_L/D_{app} - 1$ against θ_L^0:

$$\frac{D_L}{D_{app}} - 1 = 3K_T\frac{N_T}{N_L}\left[\frac{1}{K_T\theta_L^0} + \frac{2}{(K_T\theta_L^0)^2} - \frac{2}{(K_T\theta_L^0)^3}(1+K_T\theta_L^0)\ln(1+K_T\theta_L^0)\right] \quad (25)$$

This expression, equation (10) in the original reference [24], is here rearranged and variables are renamed following a more familiar nomenclature for trapping modelling. The curve is fitted in Matlab implementing the custom equation and using a non-linear least squares algorithm. Trapping values are found to be: $E_B = 27.12$ kJ/mol and $N_T = 3.67 \times 10^{25}$ traps/m^3.

Uptake constants

Following the uptake theory presented in section 3.4.2 a simplified procedure is followed to find constants. To summarize.

(1)the ratio $\kappa_{HAR} = k_{abs}/k_{des}$ is fixed as 10^{-6} [40] and $k_{abs} = 1$ m/s

(2)the surface coverage θ_{ad} is found assuming that $k_{des} \gg J_{in}$:

$$C_L^0 = N_L\frac{k_{abs}}{k_{des}}\frac{\theta_{ad}}{1-\theta_{ad}} \quad (26)$$

where $C_L^0 = J_{ss}L/D_L$ and $J_{ss} = i_{ss}/F$.

(3) the charging constant k_c is found from the charging current and θ_{ad} using the Volmer current expression:

$$k_c = \frac{i_c}{F(1-\theta_{ad})} \quad (27)$$

(4)The ratio κ_{HER} and $k_{r,ch}$ are found assuming $k_c \gg J_{in}$:

$$\frac{\theta_{ad}^2}{1-\theta_{ad}} = \frac{k_{r,ch}}{k_c} = \frac{1}{\kappa_{HER}} \quad (28)$$

All results of fitted electrochemical constants are shown in Tables 5–7 following the procedure described above. It has been demonstrated that only the ratio κ_{HAR} influences the magnitude of $k_{r,ch}$, k_c and θ_{ad} but not the particular choice of

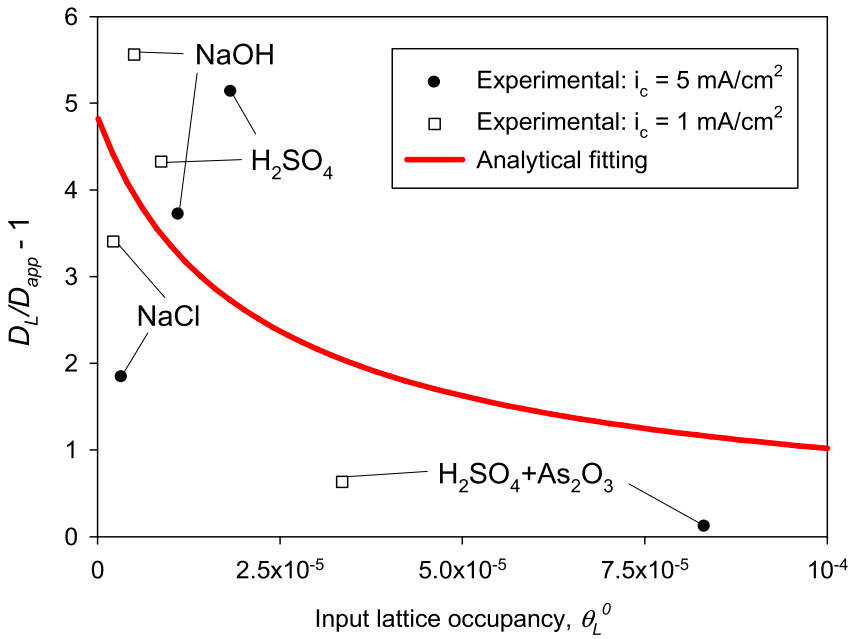

Fig. 15 – Mapping of trapping effects and numerical fitting (P2500).

Please cite this article as: Peral LB et al., Hydrogen uptake and diffusion kinetics in a quenched and tempered low carbon steel: experimental and numerical study, International Journal of Hydrogen Energy, https://doi.org/10.1016/j.ijhydene.2023.05.286

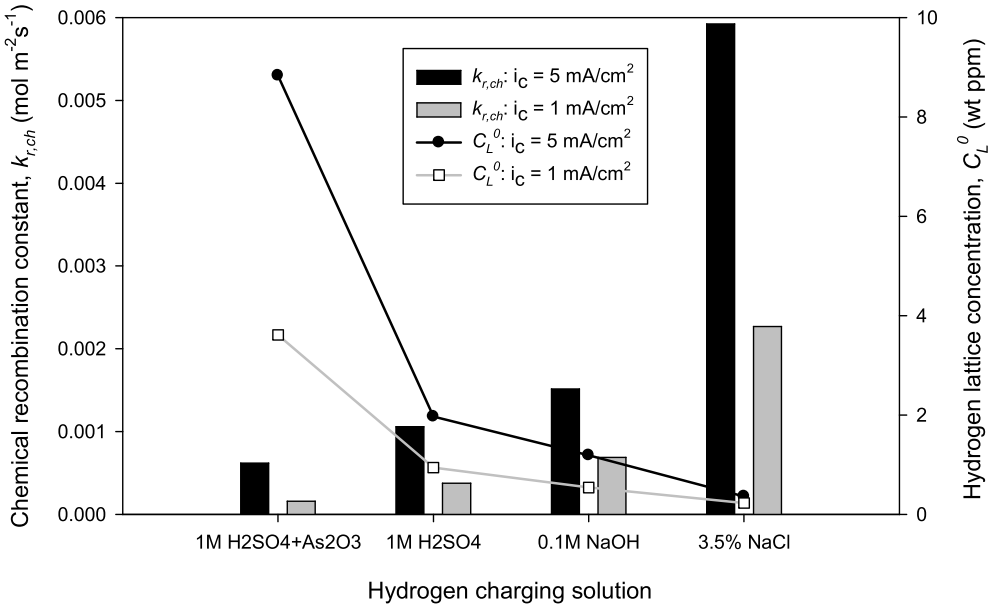

Fig. 16 – Hydrogen recombination constant ($k_{r,ch}$) fitted from permeation results for P2500.

k_{abs} or k_{des}. For a higher κ_{HAR}, lower coverage θ_{ad} and k_c values are obtained whereas the recombination constant $k_{r,ch}$ increases. A value $\kappa_{HAR} = 10^{-6}$, chosen from Turnbull et al. [40] for a Cr–Mo steel, also reproduces a coverage close to a saturation of surface sites, as predicted by Frappart et al. [12] and thus it is demonstrated as a reasonable choice.

For a rough surface, as shown in Table 5, i.e. for P120 grinding, hydrogen output flux is much lower than for lower roughness values, indicating a lower concentration on the entry side. Applying HER theory to fit electrochemical constants and surface coverage, it is found that k_c and θ_{ad} decrease for a rough surface (P120) whereas $k_{r,ch}$ increases. A very slight difference between P2500 and P600 grinding states is found. Despite the charging current density is fixed to assess the influence of surface roughness, an increase in the effective area is expected for rough samples. Assuming that the spacing between peaks, e.g. the parameter RSm, increases after polishing and the height of these peaks decreases, as demonstrated through Ra, it is expected that the equivalent surface decreases. However, to quantify the area increase the hybrid parameter Sdr (Developed Interfacial Area Ratio) should be measured, which is not available here. The use of Sdr as a predictor of coating behaviours [45] and interfaces [46] has been demonstrated to be more sensitive than height roughness parameters.

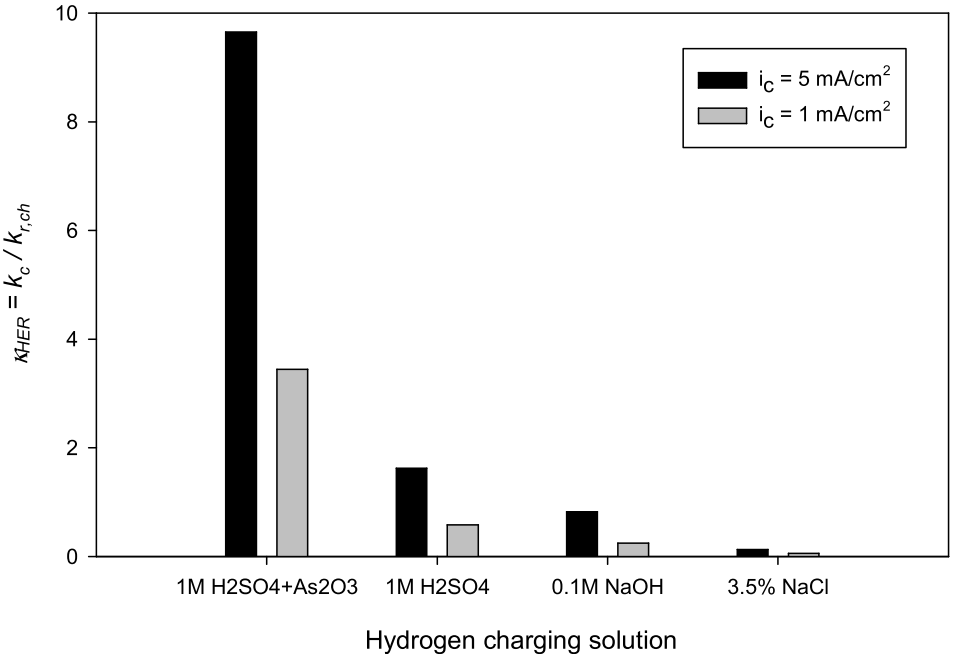

Fig. 17 – Ratio between charging and recombination constants ($\kappa_{HER} = k_c/k_{r,ch}$) fitted from permeation results for P2500.

Please cite this article as: Peral LB et al., Hydrogen uptake and diffusion kinetics in a quenched and tempered low carbon steel: experimental and numerical study, International Journal of Hydrogen Energy, https://doi.org/10.1016/j.ijhydene.2023.05.286

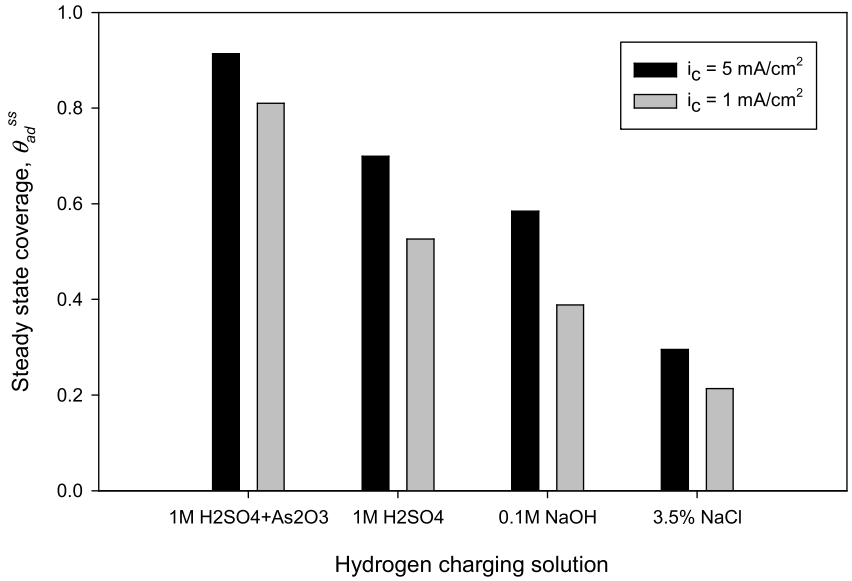

Fig. 18 – Coverage of adsorbed hydrogen at steady state (θ_{ad}^{ss}) fitted from permeation results for P2500.

Therefore, the influence of roughness is double-fold: (i) rough surface corresponds to a larger area and therefore the effective charging current density is lower than the nominal applied value This explains partly the increase in hydrogen adsorption, and thus in k_c, after polishing; however, it must be noted that the exit side is grinded at the same level than the entry surface and the area effect could then be balanced. (ii) Recombination is influenced not only by the effective area but

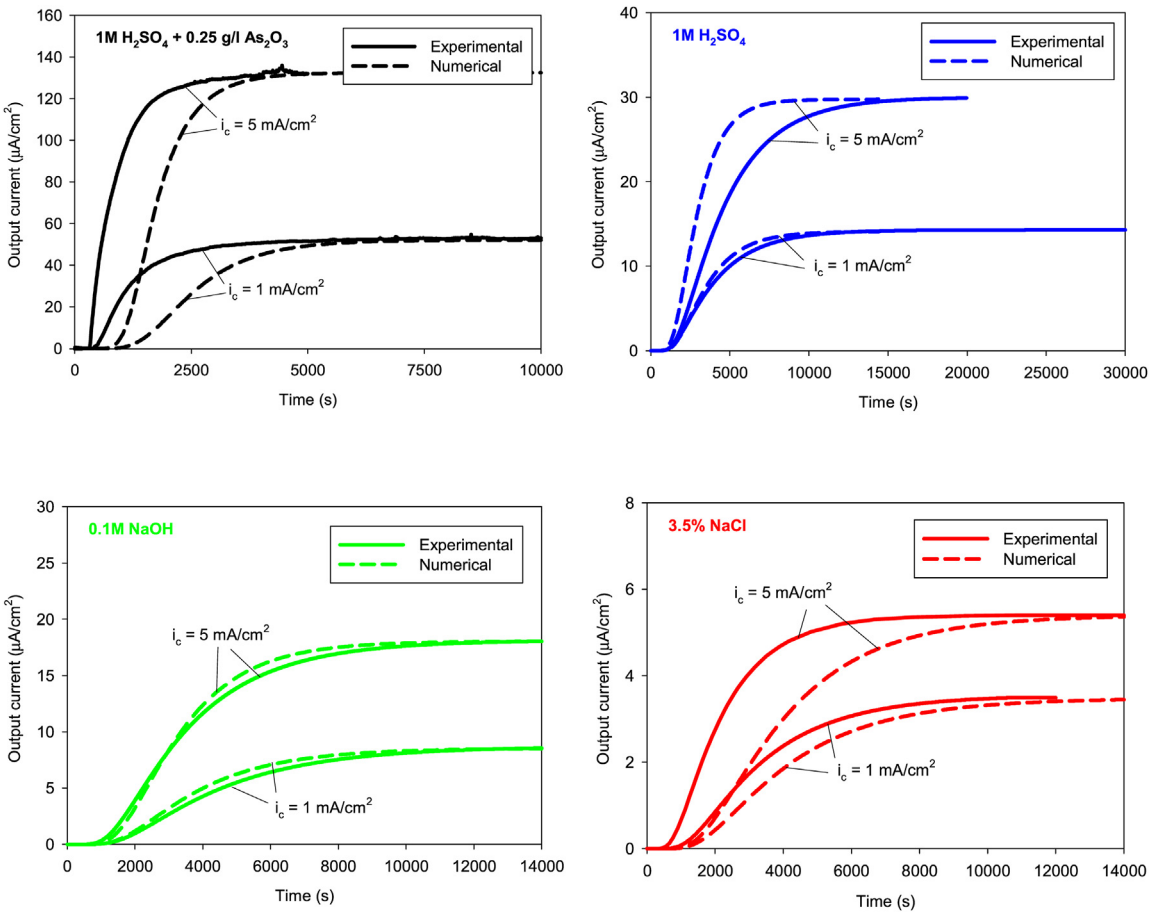

Fig. 19 – Comparison of experimental and numerical permeation transients for different charging solutions and P2500. The fitted trapping values (E_B = 27.12 kJ/mol and N_T = 3.67 × 10^{25} traps/m^3) are considered.

Please cite this article as: Peral LB et al., Hydrogen uptake and diffusion kinetics in a quenched and tempered low carbon steel: experimental and numerical study, International Journal of Hydrogen Energy, https://doi.org/10.1016/j.ijhydene.2023.05.286

an effect of surface morphology is expected. This can be observed since not only k_c is affected by the roughness level but also the recombination constant $k_{r,ch}$; the ratio κ_{HER}, which quantifies the efficiency in hydrogen adsorption, clearly increases after polishing.

The analysis of uptake parameters for P2500, two different charging currents (1 and 5 mA/cm^2) and four different electrolytes is included in Tables 6, 7. Using the experimental lattice diffusivity D_L, steady state output currents can be translated into an input lattice concentration on the entry side C_L^0. It must be noted that the expression $C_L^0 = J_{ss}L/D_L$ assumes a triangular distribution of C_L through the thickness at the steady state. Therefore, a higher i_{ss} produces a higher C_L^0 and, assuming equation (26), a higher surface coverage θ_{ad}. This fact explains that the surface coverage increases with the charging current, i.e. it is higher for 5 than for 1 mA/cm^2, and also for the electrolytes with a higher charging current k_c. It is experimentally verified that k_c increases for acid media, i.e. it is proportional to C_{H^+} as described in Section 3.3. Volmer and Tafel constants or charge transfer coefficients are not assessed, and thus the higher κ_{HER} and consequently higher θ_{ad} is only attributed to the different concentration of protons in the charging electrolyte. On the other, the chemical recombination constant increases for a charging current of 5 mA/cm^2 and for the electrolytes showing a lower output current i_{ss}, as expected. In Fig. 16, the recombination constant, $k_{r,ch}$, and the lattice concentration on the entry side, C_L^0, are plotted, also demonstrating the poisoning effect of As_2O_3 in hydrogen recombination. Additionally, the constant κ_{HER}, which can be regarded as an indicator of adsorption efficiency, is much higher for the charging solution 1 M H_2SO_4 + 0.25 g/l As_2O_3, as shown in Fig. 17. The high values of the surface coverage θ_{ad} are produced by the assumed low $\kappa_{HAR} = k_{abs}/k_{des}$, which reproduces a desorption much faster than absorption and therefore even low C_L^0 values are related to saturated surface sites. Surface coverage, as shown in Fig. 18, ranges from 0.2 for 3.5% NaCl to 0.9 for 1 M H_2SO_4 + 0.25 g/l As_2O_3.

Finite element verification

In this section permeation curves are numerically reproduced in Comsol Multiphysics 6.0 to validate the fitting procedure for uptake constants. To that purpose, generalized boundary conditions from HER and HAR reactions are implemented in the entry flux, while the bulk material is modelled considering diffusion and trapping equations detailed in Section 3.4.1. In Fig. 19, it is observed that a good agreement between experimental and numerical curves is obtained only for some conditions, e.g. 1 M H_2SO_4 or 3.5% NaCl at 1 mA/cm^2 or for 0.1 M NaOH for both charging conditions. The deviation in other curves is explained by the scatter in the mapping fitting procedure to determine N_T and E_B values that are independent of the charging electrolyte or current. For instance, since both experimental points for 1 M H_2SO_4 + 0.25 g/l As_2O_3 lie below the fitted curve (Fig. 15), the D_{app} numerically reproduced is

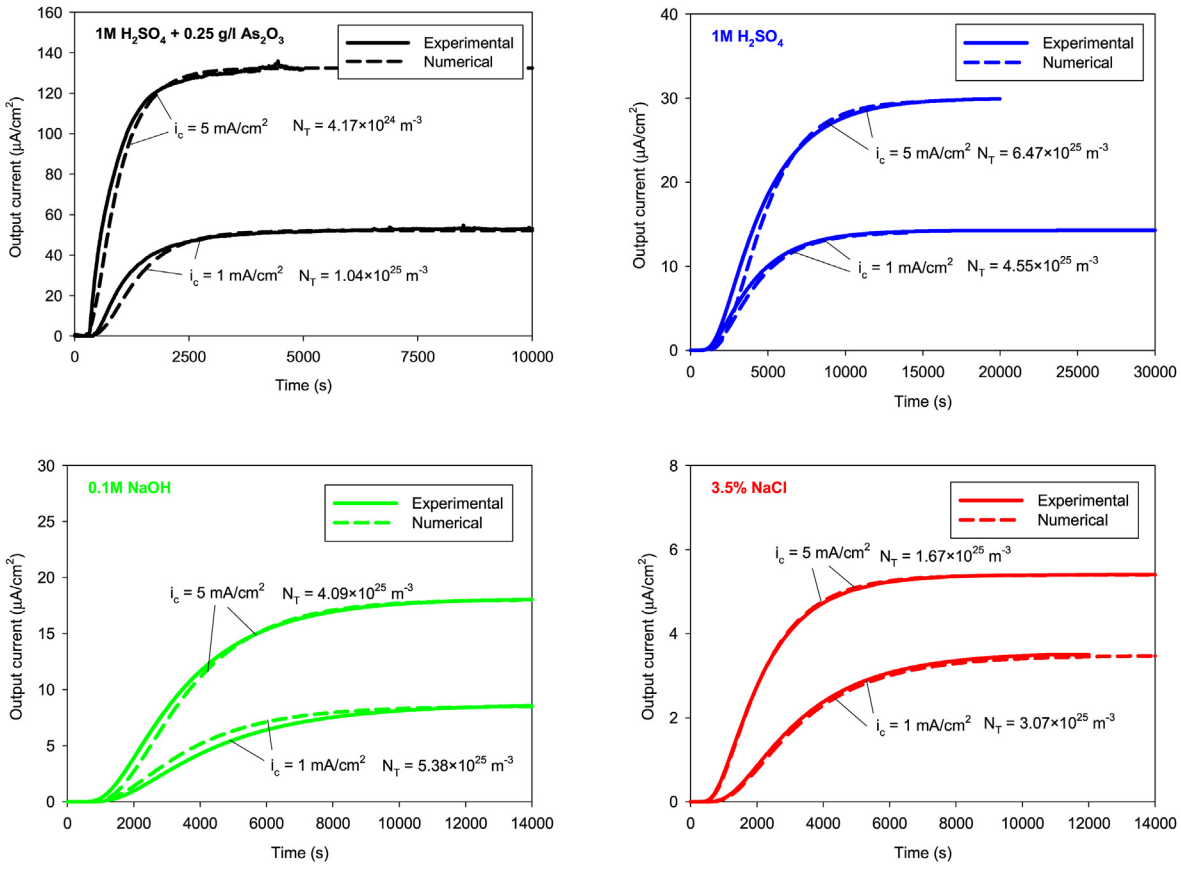

Fig. 20 – Comparison of experimental and numerical permeation transients for different charging solutions and P2500. The fitted binding energy (E_B = 27.12 kJ/mol) and individually fitted trapping densities are considered.

Please cite this article as: Peral LB et al., Hydrogen uptake and diffusion kinetics in a quenched and tempered low carbon steel: experimental and numerical study, International Journal of Hydrogen Energy, https://doi.org/10.1016/j.ijhydene.2023.05.286

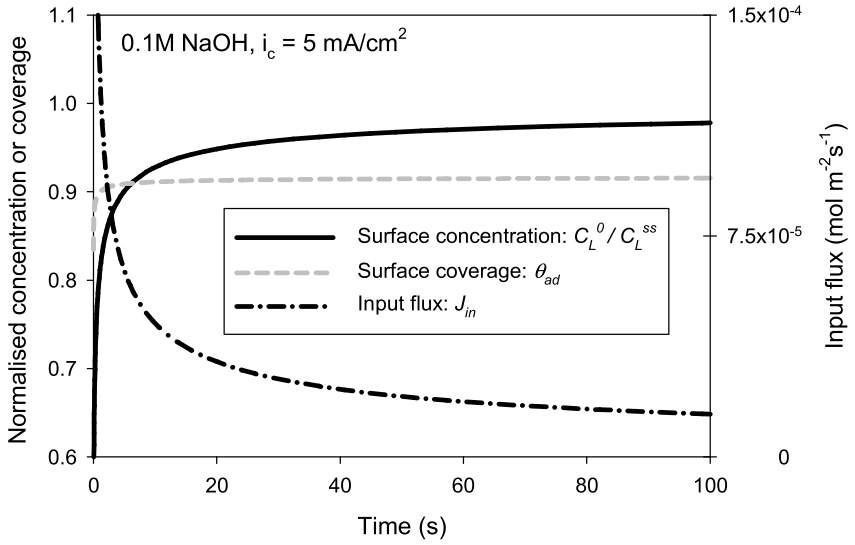

Fig. 21 – Simulated evolution of hydrogen concentration, surface coverage and input flux on the entry side for 0.1NaOH, 5 mA/cm² and P2500.

lower than the particular apparent diffusivity for those tests. This is demonstrated by fixing the binding energy with the fitted value, i.e. 27.12 kJ/mol, and iterating over the N_T value until the analytical solution in Fig. 15 matches each individual test point. These individually fitted curves are shown in Fig. 20. Anyway, N_T values reported in this work, in the order of 10^{25} sites/m^3, are in agreement with [47] where N_T values of 10^{23}-10^{26} sites/m^3 have been typically associated to hydrogen trapping sites in martensitic steels. Trapping binding energies, E_b, in the range of 25–30 kJ/mol are commonly associated with the elastic-field of dislocations in tempered martensitic steels [48].

It must be highlighted that Condition 1 and 2 (Section 3.4.2) are only required to determine constants from permeation results, but the numerical boundary conditions implemented in Comsol Multiphysics do not assume any simplification and they can reproduce both surface-controlled and diffusion-controlled situations.

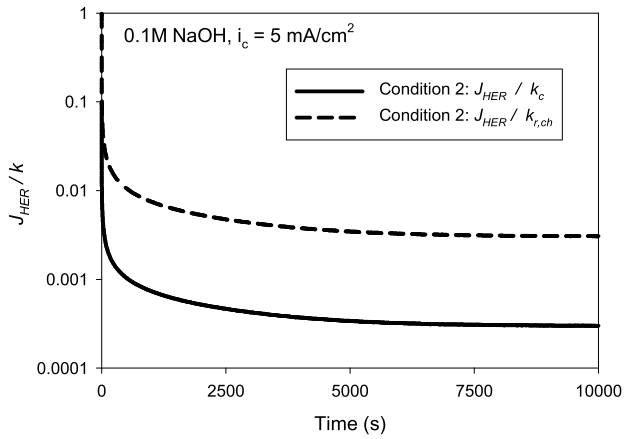

Fig. 22 – Verification of Condition 2 ($J_{HER} \ll k_c$ and $J_{HER} \ll k_{r,ch}$) for 0.1NaOH, 5 mA/cm² and P2500.

The boundary values of concentration and flux are also assessed for the permeation simulations reproduced in Fig. 21. The generalized boundary conditions here implemented model a transient entry flux, J_{in}, from the reaction balance $J_{HER} = J_{HAR}$, where HAR flux is a function of C_L^0 and thus the assumption of constant concentration or constant flux are no longer valid. However, as shown in Fig. 20 for the particular case of 0.1 M NaOH at 5 mA/cm^2, hydrogen concentration at the entry surface reaches a constant value after approximately 100 s while the input flux still decreases. The surface coverage θ_{ad} also increases at the first stages of permeation but the stabilization time is lower in this case. The validity range of a constant concentration, and thus of the fitting procedure to find k_c, $k_{r,ch}$ and θ_{ad}, is related to Conditions 1 and 2 defined in Section 3.4.2. Condition 1 is not plotted because $J_{HAR}/(N_L k_{abs})$, and so $J_{HAR}/(N_L k_{des})$, is lower than 10^{-3} even at the first stages of hydrogen entry. However, Condition 2 is not verified during the first seconds of permeation as shown in Fig. 22, i.e. $J_{HER} \ll k_c$ or $J_{HER} \ll k_{r,ch}$ cannot be assumed. This high flux J_{HER} results in the deviation from constant θ_{ad} and therefore from constant C_L^0 at short times, when concentration gradients are large [40].

Conclusions

After analyzing the electrochemical permeation experiments conducted on a low alloy steel, the following conclusions can be drawn:

Surface roughness notably influences hydrogen uptake. This fact is associated to hydrogen adsorption/desorption mechanisms, simulated from the hydrogen evolution reaction (HER). P120 state (i.e. rough surface) showed a lower hydrogen concentration on the entry side in comparison to P600 and P2500 states. However, subsurface hydrogen concentration and consequently, the apparent diffusivity increased for P600

Please cite this article as: Peral LB et al., Hydrogen uptake and diffusion kinetics in a quenched and tempered low carbon steel: experimental and numerical study, International Journal of Hydrogen Energy, https://doi.org/10.1016/j.ijhydene.2023.05.286

and P2500 grinding states due to the lower chemical recombination constant ($k_{r,ch}$) that exists for the smoothest surfaces.

After studying the different hydrogen charging solutions, the apparent diffusivity evolves as a function of the apparent hydrogen concentration. Two domains, which are associated with a competition between hydrogen trapping and hydrogen lattice diffusion, were identified. In addition, hydrogen charging and recombination constants have been fitted from permeation results following HER theory and assuming a fixed value for the ratio between absorption and desorption constants. Hydrogen chemical recombination was notably reduced due to the As_2O_3 addition to the 1 M H_2SO_4 charging solution. Hence, higher hydrogen concentrations were introduced at the subsurface level. This fact was mainly evidenced at $i_c = 5$ mA/cm^2, where interstitial diffusivity seems to prevail (with $D_L \approx D_{app}$). However, chemical recombination increased in 1 M H_2SO_4, being this effect especially notable in the electrochemical permeation tests carried out in 3.5% NaCl. In these cases, the effect of trapping and detrapping kinetics was dominant (with $D_L > D_{app}$).

Finally, considering the fitted uptake constants, a 1D finite element framework has been developed in Comsol Multiphysics to reproduce hydrogen permeation. This model includes hydrogen trapping effects and requires two trapping parameters, i.e. a binding energy and a trap density, that are independent of the surface conditions and have been fitted following a mapping strategy. On the other hand, generalized boundary conditions have been implemented to reproduce entry fluxes from HER and absorption theory. Numerical predictions of hydrogen uptake and permeation transients for all the tested charging conditions agree with the experimental results despite some deviations are found due to the experimental scatter in trapping fitting.

Data availability statement

The data that sustain the findings of this study are available from the corresponding author, prior reasonable request.

Declaration of competing interest

The authors declare that they have no known competing financial interests or personal relationships that could have appeared to influence the work reported in this paper.

Acknowledgments

The authors would like to thank the Spanish Government for the financial support received to perform the research projects RTI2018-096070-B-C33 and PID2021-124768OB-C21. This work was supported by the Regional Government of Castilla y León (Junta de Castilla y León) and by the Ministry of Science and Innovation MICIN and the European Union Next Generation EU/PRTR (MR4W.P2 and MR5W.P3). L.B. Peral is also grateful for his Margarita Salas Postdoctoral contract (Ref.: MU-21-UP2021-030) funded by the University of Oviedo through the Next Generation European Union.

REFERENCES

[1] Oliveira AM, Beswick RR, Yan Y. A green hydrogen economy for a renewable energy society. Curr Opin Chem Eng 2021;33. https://doi.org/10.1016/j.coche.2021.100701.
[2] Ishaq H, Dincer I, Crawford C. A review on hydrogen production and utilization: challenges and opportunities. Int J Hydrogen Energy 2022;47:26238–64. https://doi.org/10.1016/j.ijhydene.2021.11.149.
[3] Matsunaga H, Yoshikawa M, Kondo R, Yamabe J, Matsuoka S. Slow strain rate tensile and fatigue properties of Cr-Mo and carbon steels in a 115 MPa hydrogen gas atmosphere. Int J Hydrogen Energy 2015;40:5739–48. https://doi.org/10.1016/j.ijhydene.2015.02.098.
[4] Hua Z, Zhang X, Zheng J, Gu C, Cui T, Zhao Y, Peng W. Hydrogen-enhanced fatigue life analysis of Cr–Mo steel high-pressure vessels. Int J Hydrogen Energy 2017;42:12005–14. https://doi.org/10.1016/j.ijhydene.2017.02.103.
[5] Tsuda K, Kimura S, Takaki T, Toyofuku Y, Adaniya K, Shinto K, Miyoshi K, Hirata K, Christiani L, Takada M, Kobayashi N, Baba S, Nagamatsu Y, Takata M. Design proposal for hydrogen refueling infrastructure deployment in the Northeastern United States. Int J Hydrogen Energy 2014;39:7449–59. https://doi.org/10.1016/j.ijhydene.2014.03.002.
[6] Alazemi J, Andrews J. Automotive hydrogen fuelling stations: an international review. Renew Sustain Energy Rev 2015;48:483–99. https://doi.org/10.1016/j.rser.2015.03.085.
[7] Moshtaghi M, Safyari M, Mori G. Combined thermal desorption spectroscopy, hydrogen visualization, HRTEM and EBSD investigation of a Ni–Fe–Cr alloy: the role of hydrogen trapping behavior in hydrogen-assisted fracture. Mater Sci Eng 2022;848. https://doi.org/10.1016/j.msea.2022.143428.
[8] Vandewalle L, Konstantinović MJ, Verbeken K, Depover T. A combined thermal desorption spectroscopy and internal friction study on the interaction of hydrogen with microstructural defects and the influence of carbon distribution. Acta Mater 2022;241:118374. https://doi.org/10.1016/j.actamat.2022.118374.
[9] Peral LB, Zafra A, Fernández-Pariente I, Rodríguez C, Belzunce J. Effect of internal hydrogen on the tensile properties of different CrMo(V) steel grades: influence of vanadium addition on hydrogen trapping and diffusion. Int J Hydrogen Energy 2020;45:22054–79. https://doi.org/10.1016/j.ijhydene.2020.05.228.
[10] Peral LB, Amghouz Z, Colombo C, Fernández-Pariente I. Evaluation of hydrogen trapping and diffusion in two cold worked CrMo(V) steel grades by means of the electrochemical hydrogen permeation technique. Theor Appl Fract Mech 2020;110:102771. https://doi.org/10.1016/j.tafmec.2020.102771.
[11] Zafra A, Peral LB, Belzunce J. Hydrogen diffusion and trapping in A 42CrMo4 quenched and tempered steel: influence of tempering temperature. Int J Hydrogen Energy 2020;45:31225–42. https://doi.org/10.1016/j.ijhydene.2020.08.134.
[12] Frappart S, Feaugas X, Creus J, Thebault F, Delattre L, Marchebois H. Study of the hydrogen diffusion and segregation into Fe–C–Mo martensitic HSLA steel using electrochemical permeation test. J Phys Chem Solid 2010;71:1467–79. https://doi.org/10.1016/j.jpcs.2010.07.017.
[13] ASTMG148-97. Standard practice for evaluation of hydrogen uptake, permeation, and transport in metals by an electrochemical technique. 2018.

Please cite this article as: Peral LB et al., Hydrogen uptake and diffusion kinetics in a quenched and tempered low carbon steel: experimental and numerical study, International Journal of Hydrogen Energy, https://doi.org/10.1016/j.ijhydene.2023.05.286

[14] el Alami H, Creus J, Feaugas X. Influence of the plastic strain on the hydrogen evolution reaction on polycrystalline nickel electrodes in H2S04. Electrochim Acta 2006;51:4716–27. https://doi.org/10.1016/j.electacta.2006.01.012.
[15] Takasawa K, Ikeda R, Ishikawa N, Ishigaki R. Effects of grain size and dislocation density on the susceptibility to high-pressure hydrogen environment embrittlement of high-strength low-alloy steels. Int J Hydrogen Energy 2012;37:2669–75. https://doi.org/10.1016/j.ijhydene.2011.10.099.
[16] Zhang S, Huang Y, Sun B, Liao Q, Lu H, Jian B, Mohrbacher H, Zhang W, Guo A, Zhang Y. Effect of Nb on hydrogen-induced delayed fracture in high strength hot stamping steels. Mater Sci Eng, A 2015;626:136–43. https://doi.org/10.1016/j.msea.2014.12.051.
[17] Zhang S, Xu D, Huang F, Gao W, Wan J, Liu J. Mitigation of hydrogen embrittlement in ultra-high strength lath martensitic steel via Ta microalloying. Mater Des 2021;210:110090. https://doi.org/10.1016/j.matdes.2021.110090.
[18] Peral LB, Fernández-Pariente I, Colombo C, Rodríguez C, Belzunce J. The positive role of nanometric molybdenum–vanadium carbides in mitigating hydrogen embrittlement in structural steels. Materials 2021;14:7269. https://doi.org/10.3390/ma14237269.
[19] Colombo C, Fumagalli G, Bolzoni F, Gobbi G, Vergani L. Fatigue behavior of hydrogen pre-charged low alloy Cr–Mo steel. Int J Fatig 2016;83:2–9. https://doi.org/10.1016/j.ijfatigue.2015.06.002.
[20] Shinko T, Halm D, Benoit G, Hénaff G. Controlling factors and mechanisms of fatigue crack growth influenced by high pressure of gaseous hydrogen in a commercially pure iron. Theor Appl Fract Mech 2021;112:102885. https://doi.org/10.1016/j.tafmec.2020.102885.
[21] Peral LB, Zafra A, Blasón S, Rodríguez C, Belzunce J. Effect of hydrogen on the fatigue crack growth rate of quenched and tempered CrMo and CrMoV steels. Int J Fatig 2019;120:201–14. https://doi.org/10.1016/j.ijfatigue.2018.11.015.
[22] Djukic MB, Bakic GM, Sijacki Zeravcic V, Sedmak A, Rajicic B. The synergistic action and interplay of hydrogen embrittlement mechanisms in steels and iron: localized plasticity and decohesion. Eng Fract Mech 2019;216:106528. https://doi.org/10.1016/j.engfracmech.2019.106528.
[23] Sofronis P, McMeeking RM. Numerical analysis of hydrogen transport near a blunting crack tip. J Mech Phys Solid 1989;37:317–50. https://doi.org/10.1016/0022-5096(89)90002-1.
[24] McNabb A, Foster PK. A new analysis of the diffusion of hydrogen in iron and ferritic steels. Trans Metall Soc AIME 1963;227:618–27. citeulike-article-id:4956272.
[25] Caskey GR, Pillinger WL. Effect of trapping on hydrogen permeation. Metall Trans A 1975;6:3(6):467–76. https://doi.org/10.1007/BF02658404.
[26] Kumnick AJ, Johnson HH. Deep trapping states for hydrogen in deformed iron. Acta Metall 1980;28:33–9. https://doi.org/10.1016/0001-6160(80)90038-3.
[27] Oriani RA. The diffusion and trapping of hydrogen in steel. Acta Metall 1970;18:147–57. https://doi.org/10.1016/0001-6160(70)90078-7.
[28] Raina A, Deshpande VS, Fleck NA. Analysis of electro-permeation of hydrogen in metallic alloys. Philos Trans A Math Phys Eng Sci 2017;375:20160409. https://doi.org/10.1098/rsta.2016.0409.
[29] Díaz A, Cuesta II, Martinez-Pañeda E, Alegre JM. Analysis of hydrogen permeation tests considering two different modelling approaches for grain boundary trapping in iron. Int J Fract 2020;223:17–35. https://doi.org/10.1007/S10704-019-00411-8/FIGURES/19.
[30] Montella C. Discussion on permeation transients in terms of insertion reaction mechanism and kinetics. J Electroanal Chem 1999;465:37–50. https://doi.org/10.1016/S0022-0728(99)00051-0.
[31] Martínez-Pañeda E, Díaz A, Wright L, Turnbull A. Generalised boundary conditions for hydrogen transport at crack tips. Corrosion Sci 2020;173:108698. https://doi.org/10.1016/j.corsci.2020.108698.
[32] N. Parvathavarthini, S. Saroja, R.K. Dayal, H.S. Khatak, Studies on hydrogen permeability of 2.25% Cr±1% Mo ferritic steel: correlation with microstructure, n.d. www.elsevier.nl/locate/jnucmat.
[33] Pillot S, Coudreuse L. Hydrogen-induced disbonding and embrittlement of steels used in petrochemical refining. In: Gaseous hydrogen embrittlement of materials in energy technologies. Elsevier; 2012. p. 51–93. https://doi.org/10.1533/9780857093899.1.51.
[34] Liu Q, Atrens AD, Shi Z, Verbeken K, Atrens A. Determination of the hydrogen fugacity during electrolytic charging of steel. Corrosion Sci 2014;87:239–58. https://doi.org/10.1016/J.CORSCI.2014.06.033.
[35] Turnbull A. Perspectives on hydrogen uptake, diffusion and trapping. Int J Hydrogen Energy 2015;40:16961–70. https://doi.org/10.1016/j.ijhydene.2015.06.147.
[36] Díaz A, Zafra A, Martínez-Pañeda E, Alegre JM, Belzunce J, Cuesta II. Simulation of hydrogen permeation through pure iron for trapping and surface phenomena characterisation. Theor Appl Fract Mech 2020;110:102818. https://doi.org/10.1016/j.tafmec.2020.102818.
[37] Dadfarnia M, Sofronis P, Neeraj T. Hydrogen interaction with multiple traps: can it be used to mitigate embrittlement? Int J Hydrogen Energy 2011;36:10141–8. https://doi.org/10.1016/j.ijhydene.2011.05.027.
[38] Rodchenkova NI, Zaika YV. Numerical modelling of hydrogen desorption from cylindrical surface. Int J Hydrogen Energy 2011;36:1239–47. https://doi.org/10.1016/J.IJHYDENE.2010.06.121.
[39] Zaika YV, Kostikova EK. Computer simulation of hydrogen thermal desorption by ODE-approximation. Int J Hydrogen Energy 2017;42:405–15. https://doi.org/10.1016/J.IJHYDENE.2016.10.104.
[40] Turnbull A, Ferriss DH, Anzai H. Modelling of the hydrogen distribution at a crack tip. Mater Sci Eng, A 1996;206:1–13. https://doi.org/10.1016/0921-5093(95)09897-6.
[41] Réquiz R, Vera N, Camero S. The influence of surface roughness on the hydrogen permeation of type API 5L-X52 steel. Rev. Metal. Madrid. 2004;40:30–8.
[42] Zakroczymski T. Adaptation of the electrochemical permeation technique for studying entry, transport and trapping of hydrogen in metals. Electrochim Acta 2006:2261–6. https://doi.org/10.1016/j.electacta.2005.02.151.
[43] Fallahmohammadi E, Bolzoni F, Fumagalli G, Re G, Benassi G, Lazzari L. Hydrogen diffusion into three metallurgical microstructures of a C-Mn X65 and low alloy F22 sour service steel pipelines. In: Int J hydrogen energy. Elsevier Ltd; 2014. p. 13300–13. https://doi.org/10.1016/j.ijhydene.2014.06.122.
[44] Dogan H, Li D, Scully JR. Controlling hydrogen embrittlement in precharged ultrahigh-strength steels. Corrosion 2007;63:689–703. https://doi.org/10.5006/1.3278418.
[45] Eliaz N, Shmueli S, Shur I, Benayahu D, Aronov D, Rosenman G. The effect of surface treatment on the surface texture and contact angle of electrochemically deposited hydroxyapatite coating and on its interaction with bone-forming cells. Acta Biomater 2009;5:3178–91. https://doi.org/10.1016/J.ACTBIO.2009.04.005.

Please cite this article as: Peral LB et al., Hydrogen uptake and diffusion kinetics in a quenched and tempered low carbon steel: experimental and numerical study, International Journal of Hydrogen Energy, https://doi.org/10.1016/j.ijhydene.2023.05.286

[46] van Dam JPB, Abrahami ST, Yilmaz A, Gonzalez-Garcia Y, Terryn H, Mol JMC. Effect of surface roughness and chemistry on the adhesion and durability of a steel-epoxy adhesive interface. Int J Adhesion Adhes 2020;96:102450. https://doi.org/10.1016/J.IJADHADH.2019.102450.
[47] Shi R, Chen L, Wang Z, Yang X-S, Qiao L, Pang X. Quantitative investigation on deep hydrogen trapping in tempered martensitic steel. J Alloys Compd 2021;854:157218. https://doi.org/10.1016/j.jallcom.2020.157218.
[48] Colombo C, Zafra García A, Belzunce J, Fernandez Pariente I. Sensitivity to hydrogen embrittlement of AISI 4140 steel: a numerical study on fracture toughness. Theor Appl Fract Mech 2020;110. https://doi.org/10.1016/j.tafmec.2020.102810.

Please cite this article as: Peral LB et al., Hydrogen uptake and diffusion kinetics in a quenched and tempered low carbon steel: experimental and numerical study, International Journal of Hydrogen Energy, https://doi.org/10.1016/j.ijhydene.2023.05.286